Purification and initial structural characterization of AlfA, a novel bacterial actin necessary for plasmid segregation

by

Shun Kai Yang ©
Department of Anatomy and Cell Biology
McGill University, Montreal

A thesis submitted to McGill University in partial fulfillment of the requirements for the Degree of Master of Science in Anatomy and Cell Biology

on

Table of Content

Abstract (English)

Eukaryotic actins are involved in many important processes in the cell, but how they evolved from prokaryotic actins remains unclear. Previous research shows that one of these bacterial actins, actin-like-filament-A (AlfA) shares many characteristics with eukaryotic actin. AlfA is capable of forming filamentous structures, which segregate plasmids in *Bacillus subtilis natto* during cell division. Research on AlfA may help to explicate the evolutionary link between these two actin families. To accomplish this objective, a high-resolution structure of the AlfA filament by X-ray crystallography would provide a better understanding of AlfA structure. Additionally, biochemical studies and functional assays will elucidate the function and dynamics of AlfA.

Initially, we optimized the purification of AlfA using a novel expression approach to generate purified protein in quantities sufficient for structural characterization. AlfA mutants were generated to help define the polymerization interfaces, and our biochemical studies and EM micrographs showed that R78D/K79D mutants are polymerization incompetent. We have begun crystallizing AlfA and mutants for X-ray analysis, and one of the crystal hits was optimized using additive screen to produce hexagonal crystals. Our functional assays *in vivo* revealed that the truncation of AlfA resulted in plasmid DNA loss. Our results suggest that AlfA polymerization is required for ensuring plasmid inheritance.

Our long-term goal is to generate an accurate model of the filament by docking a high-resolution crystal structure into a medium resolution cryo-EM structure. This may enhance our understanding of how eukaryotic actins were evolved, and aid developing new pharmaceuticals to target the segregation of virulence plasmids in multidrug-resistant bacteria.

Abstract (Français)

Les actines eucaryotiques sont impliqués dans de nombreux processus cellulaires. Même si elles ont été extensivement étudiées, peu est compris quant à leur évolution à partir des actines procaryotiques. Actin-like filament A (AlfA) est une actine bactérienne comprenant des caractéristiques semblables aux actines eucaryotiques. AlfA forme des structures filamenteuses pour ségréguer les plasmides de *Bacillus subtilis natto* lors de sa fission cellulaire. L'étude d'AlfA pourrait élucider le lien évolutionnaire entre les actines eucaryotiques et procaryotiques. Or, une structure à haute résolution obtenue par cristallographie aux rayons X, ainsi que des études biochimiques et structurelles permettront de mieux comprendre la structure et la fonction d'AlfA.

Nous avons optimisé la purification d'AlfA en utilisant une nouvelle méthode d'expression avec un rendement suffisant pour la caractérisation structurale. Des mutations dans AlfA ont aidé à établir les interfaces de polymérisation. À l'aide d'études biochimiques et de visualisions de micrographes par microscope électronique, nous avons déterminé que les mutations à R78D/K79D empêchent la polymérisation d'AlfA. Nos tentatives de cristallisation d'AlfA et ses mutants ont été initiées, et l'optimisation d'un cristal a débuté, résultant avec des cristaux hexagonaux. La troncation d'AlfA in vivo résulte en une perte d'ADN, démontrant la nécessité de la polymérisation d'AlfA pour la transmission de plasmides.

Nous désirons obtenir un modèle précis des filaments par amarrage d'une structure à haute résolution dans une à résolution moyenne obtenue par cryomicroscopie électronique. Cela aidera à comprendre l'évolution des actines et permettra le développement de médicaments ciblant la ségrégation de plasmides virulents dans les bactéries.

Acknowledgments

Special thanks for Dr. Justin Kollman (McGill University & University of Washington) for his guidance and patience in the past two years - big hugs for him. Mr. Jesse Hansen for helps with purification, cloning, and fun times together. Also Dr. Bhushan Nagar and Yazan Abbas for supervising and guiding with the crystallography aspect of this project. Dr. Craig Mandato for being an awesome supervisor and all of the free lunches. Dr. Kalle Gehring for taking the time and efforts to review this thesis. Other members of the committee: Dr. Chantal Autexier for being kind and sweet, and Dr. Isabelle Rouiller for giving advices on EM. Thanks to FEMR for their electron microscopes, especially Dr. Kautuv Basu who never hesitated to offer assistance despite of his son sick. Also would like to acknowledge lab members Emeric Charles, Gülsima Usler, Dr. Nancy Hom and our collaborator Dr. Jessica Polka and Dr. Dyche Mullins for previous works on the AlfA project, and other members of the lab, including Dr. Elizabeth Lawrence, Dr. Khanh Huy Bui, Jason Lapointe, Matt Sheperd, and Avital Horowitz for their emotional support. Thanks for members of the department who attended the research seminars or helped with other aspects of this project (especially Joelle Denomy for administration, Melie Pagliuzza for lab chemicals and ÄKTA, And Dr. Reyes for MG1655 and PY79 cells).

In addition, acknowledgement goes out to Ahmad Gebai for translating the abstract into French. For funding, Dr. Justin Kollman (McGill, University of Washington) supported this research from CIHR grant. Dr. Denis Faubert from Institut de recherches cliniques de Montréal (IRCM) for assistance with mass spectrometry and results analysis. Dr. Anastasia Nikolakakis from Institut national de la recherche scientifique (INRS) for mass spectrometry. Katalin Kocsis Illes for helping to design the mutagenesis experiment of pBET131. Lastly, thanks to Sarah Saboobeh, Gaetan L'Italien and Jie Chen for their encouragements in finishing this thesis, and their collective efforts in editing and proofreading.

Contributing Authors

Figure 1.3 – Dr. Justin Kollman as the contributing author for making the homology model and the figure.
Figure 1.4 – Micrographs in A and B were adapted from (Polka, Kollman, Agard, & Mullins, 2009).
Figure 1.5 – Dr. Justin Kollman as the contributing author for the reconstruction, and Jelani Clark for the protein purification.
Figure 3.4 – Dr. Denis Faubert from IRCM made Tables in C and D for mass spectrometry analysis.
Figure 4.1 – Jesse Hansen as the contributing author for designing these mutations.
Figure 5.1 – Yazan Abbas as the contributing author for taking pictures in B and C.

List of Figures and Tables

List of Abbreviations

ABPs: Actin Binding Proteins
ADP: Adenosine Diphosphate
AlfA: Actin-Like-Filament-A
AlfB: Actin-Like-Filament-B
AlfC: Actin-Like-Filament-C
AMP-PNP: Adenylyl-Imidodiphosphate
ATP: Adenosine Triphosphate
BME: β-Mercaptoethanol
Cryo-ET: Cryo-Electron Tomography
dH_2O: Distilled Water
DNA: Deoxyribonucleic Acid
DTT: Dithiothreitol
EDTA: Ethylenediaminetetraacetic Acid
EM: Electron Microscopy
F-actin: Filamentous Actin
FPLC: Fast Performance Liquid Chromatography
G-actin: Globular Actin
G.F.: Gel Filtration
GFP: Green Fluorescent Protein
GTP: Guanosine Triphosphate
IPTG: Isopropyl β-D-1-Thiogalactopyranoside
PCR: Polymerase Chain Reaction
PLA: Plasmid Loss Assay
SDS-PAGE: Sodium Dodecyl Sulphate - Polyacrylamide Gel Electrophoresis
TCEP: Tris(2-carboxyethyl)phosphine
TEM: Transmission Electron Microscopy
TIRF: Total Internal Reflection Fluorescence

Chapter 1 - Introduction

1.1 Eukaryotic and Prokaryotic Actins

Eukaryotic actins are involved in many important cellular processes, such as cell motility, contraction, and division. Eukaryotic actins can be found in either globular form as monomers (G-actin), or as filaments (F-actin). Filament polymerization and depolymerization are characteristics of actins, as G-actin monomers assemble into double stranded F-actin filaments. With the help of actin-binding proteins, F-actin becomes adapted to carry out multiple cellular functions (Becker, 2009; Dominguez & Holmes, 2011). On the contrary, prokaryotic actins are highly specialized in their functions, and the evolutionary link of prokaryotic and eukaryotic actin is unclear. Previous research showed that one of these bacterial actins, actin-like-filament-A (AlfA) shares many characteristics with eukaryotic actin (Fujii, Iwane, Yanagida, & Namba, 2010; Polka et al., 2009). Detailed research on AlfA will help to resolve the evolutionary link between these two actins, and allow better understanding of how F-actin adapted to perform multiple cellular processes on the molecular level. To do this, a high-resolution structure of AlfA is needed to provide information on the functions and polymerization dynamics of AlfA, and then this information can be used to postulate the evolutionary gap between prokaryotic and eukaryotic actins.

All actins are ATPases, so G-actin monomer can readily bind to ATP to polymerize into F-actin (Figure 1.1). F-actin polymerization proceeds with the help of Arp2/3 complex that stimulate polymer nucleation (Goode, 2001). Arp2/3 are actin-binding proteins (ABPs), which are regulatory proteins that can alter the dynamics. The ABPs also organize actin into different conformation states such as bundles, branching

filaments or networks (Figure 1.1) in order to carry out various functions such as cytoskeletal support or cell motility (Becker, 2009; Dos Remedios, 2002; Winder & Ayscough, 2005).

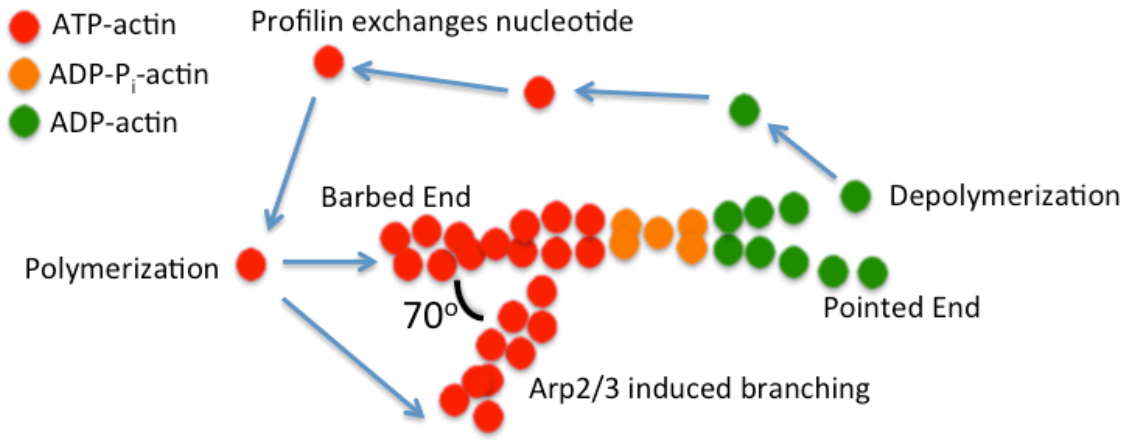

Figure 1.1. The relationship of actin polymerization, conformational states, ABPs, and functions of the ABP-actin complex.

F-actin is structurally dynamic. F-actin has polarity, and with the end with exposed nucleotide binding site called "barbed end" (Dos Remedios, 2002). Actin filament grows when additional G-actin-ATP adds on to the barbed end of the filament. On the other end of the filament (pointed end), the hydrolysis of ATP on F-actin into ADP can destabilize the filaments, thus stimulating polymer disassembly (Figure 1.1). This directional polymer growth phenomenon is know as treadmilling, and the necessity for such structural dynamics is important for F-actin functions (Winder & Ayscough, 2005). Profilin can exchange the hydrolyzed ADP into ATP, allowing continuous polymerization (Figure 1.1). F-actin is a double stranded helix with symmetry of 2.17 subunits per turn of a helix (E. H. Egelman, 2003). However, actin-binding proteins such as cofilin, which can stabilize F-actin formation, can increase the angle of turn (McGough, Pope, Chiu, & Weeds, 1997).

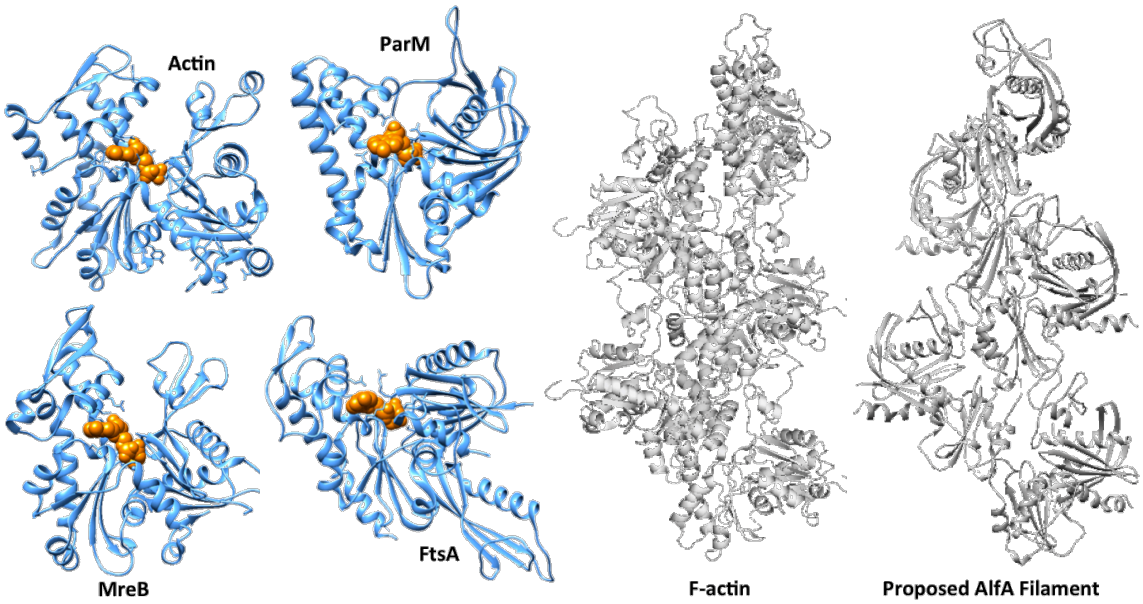

Figure 1.2. Actin and actin-like protein structures visualized using Chimera with data from previous research on actin (Otterbein, 2001), ParM (Fusinita van den Ent, Møller-Jensen, Amos, Gerdes, & Löwe, 2002), MreB (van den Ent F, 2001), FtsA (Fusinita van den Ent & Löwe, 2000), and F-actin (Galkin, Orlova, Vos, Schroder, & Egelman, 2015). Many bacterial actin homologs shared a conserved core actin fold with eukaryotic actin, allowing the hydrolysis of NTP (shown in orange spheres) to form filamentous structures.

It was traditionally thought that actin and the cytoskeleton are unique characteristics of eukaryotic cells (van den Ent F, 2001). However, prokaryotic cytoskeleton proteins share distant homology on the amino acid level. Both eukaryotic actin and prokaryotic actin share many functional features, such as the ability to polymerize into filaments, regulation of polymerization by other protein, and the formation of bundled structures by ATP binding and hydrolysis (E. Egelman, 2003; Lewis, 1992). Most importantly, the structural core of the actin subunit is largely conserved (Ozyamak, Kollman, & Komeili, 2013), and the subunit is capable of hydrolyzing nucleotide for filament polymerization (Figure 1.2). In the filamentous structure, longitudinal interactions between the protomers are also largely conserved. In general, nucleotide binding cause conformational changes

within each protomer, increasing the binding affinity between protomers to promote polymerization (Ozyamak, Kollman, & Komeili, 2013).

Prokaryotic actins retain some conserved features to eukaryotic actin, but can be organized into a diverse phylogenetic tree with many subfamilies. These actins are involved in specialized functions such as cell shape, cell division, organelle positioning, and plasmid segregation (Shaevitz & Gitai, 2010). This is different from eukaryotic actin, because eukaryotic actins interact with ABPs to perform specialized functions, and possibly imposing evolutionary constraints on eukaryotic actin. Prokaryotic actins have experienced rapid evolutionary divergence, giving rise to the diversity of structure and dynamics. This is probably because prokaryotic actins interact with fewer partners, and consequently, each bacterial actin has unique quaternary structures to assist in specialized cellular functions (Ozyamak, Kollman, & Komeili, 2013). Further analysis of unique differences in the quaternary structure will allow better understanding of how the conserved actin core functions during filament assembly and disassembly. Preliminary research has characterized a few prokaryotic actins: ParM, an actin-like protein necessary for plasmid segregation in *E. coli* (Fusinita van den Ent et al., 2002); MamK, an actin-like protein found in magnetotactic bacteria that organizes subcellular organelles called magnetosomes (Ozyamak, Kollman, Agard, & Komeili, 2013); MreB, an actin-homolog in bacteria with 15% sequence identity to actin that is responsible for cell length and cell shape (F. van den Ent, Izore, Bharat, Johnson, & Lowe, 2014). Previous research (Fig. 1.2) provids insights on the filament functions, but a higher resolution model of prokaryotic actin is needed to fully understand actin dynamics, conformational changes,

molecular mechanism of actin complexes and the evolutionary link between prokaryotic and eukaryotic actin.

Perhaps the most unique prokaryotic actin-homolog is AlfA (Actin-like-filament-A). In *Bacillus subtilis natto*, AlfA functions as a cytomotive protein for plasmid segregation during cell division. AlfA is encoded on the plasmid pLS32, separate from the host genome. Thus far, the best-understood prokaryotic model that facilitates plasmid segregation is the ParM system found in *E. coli*, but AlfA is a novel and completely different system. For example, eukaryotic actin and ParM can assemble into filaments with the addition of nucleotides, and depolymerize when ATP on the subunits becomes hydrolyzed into ADP. This constant polymerization and depolymerization (analogous to dynamic instability in microtubules) is an important feature for actin functions. However, previous TIRF microscopy data showed that AlfA does not undergo dynamic instability (Garner EC, 2004; Polka et al., 2009). Preliminary studies of AlfA monomer found that it share some conserved features with ParM and G-actin for their core actin fold (Fig. 1.2), but contrary to F-Actin filaments which assemble strictly by ATP, AlfA monomers can assemble into filaments by ATP, ADP, and GTP (Polka et al., 2009). AlfA filaments can also self-assemble into large ordered bundle structures with nucleotides, but F-actin can only do so with the presence of accessory factors. In summary, AlfA has different mechanism of polymerization from other actins, and therefore additional structural and biochemical experiments of AlfA may provide greater details about its dynamic properties during plasmid segregation.

1.2 Bacterial Plasmids

Two types of DNA are present in most bacteria: the chromosomal DNA and the plasmid DNA. Most bacteria possess double stranded chromosomal DNA in loops ranging from 160 kbp to 12.2 mbp (Nakabachi A, 2007; Pradella et al., 2002), and located in the nucleoid of the cell. The bacterial chromosomes contain most of the bacterium's genetic material necessary for bacterial functions, such as replication, growth, and survival. However, bacteria may also have one or more copies of plasmids in the cell, which are double stranded DNA that are capable of autonomous replication. Plasmids can be easily transferred from one bacterium to another or be transferred to other species via horizontal gene transfer (N. A. Campbell, 1996).

1.2.1 Function of Plasmids

Plasmids can encode genes essential for bacterial survival (Bennett, 2008; Heidelberg et al., 2002; Sengupta & Austin, 2011). Plasmid DNA can encode toxins which can cause numerous diseases and conditions (Shukla & Sharma, 2005). For example, sepsis caused by *Staphylococci* toxins affects millions of people each year in third-world countries (Shearer et al., 2011). Other prevalent life-threatening diseases caused by bacterial toxins are botulism and tetanus from the bacterial genus *Clostridium* (Marshall, 2007). Bacteria can also produce anti-toxin responsible for detoxifying heavy metals and aromatic compounds, therefore enhancing survival in heavily polluted environments (Heidelberg et al., 2002; Makarova, Wolf, & Koonin, 2009). In addition, plasmids can encode for antibiotics-resistant enzymes that can break down or inhibit antibiotics, making treatments ineffective. One example is β-lactamase to by hydrolyzing the β-lactam ring on antibiotics (Bertram Katzung, 2012). To be capable of autonomous

replication, plasmid DNA can encode actin-like proteins that facilitate the segregation of plasmids (Kenn Gerdes, 2000).

1.2.2 Plasmid Copy Number

Bacteria can possess multiple copies of the same plasmid. Plasmids small in size are maintained in high copy number. In general, high copy number plasmids create metabolic stress on the bacterium (Jones, Kim, & Keasling, 2000). However, advantages of high copy number plasmids are their capability to partition stochastically during cell division. Therefore, both daughter cells receive copies of the plasmid and the necessary genes for survival are inherited without the need for any active segregation system (del Solar, Giraldo, Ruiz-Echevarría, Espinosa, & Díaz-Orejas, 1998).

On the contrary, plasmids that are large in size are usually maintained in low copy number. In the example of pLS32, a plasmid of 85kbp size in *Bacillus subtilis natto*, is maintained at one or two copies per bacterium (Tanaka, 2010). According to Jones et al., 2000, low copy number plasmid containing bacteria achieve more cell density and faster growth rate than high copy number plasmid containing bacteria. However, a disadvantage is that large plasmid may not partition properly during cell division, in other words one of the daughter cells may not receive a copy of the plasmid. This disadvantage compromises the maintenance of plasmid in a bacterial population, and one solution has been the evolution of plasmids segregating proteins that ensure faithful inheritance of the low copy number plasmids. Since segregating proteins are directly encoded on the low copy number plasmid, they became self-sufficient cassettes to maintain the plasmid that are diverse in mechanism of action. In general, these segregating proteins can utilize

nucleotides to facilitate the translocation of plasmid with the help of adaptor proteins, which bind to the plasmids (Aylett, Wang, Michie, Amos, & Lowe, 2010; Funnell, 2003; Ozyamak, Kollman, & Komeili, 2013; J. Salje, Gayathri, & Lowe, 2010).

1.2.3 Plasmid Segregation

Several segregation mechanisms have evolved in bacteria, and are classified into Type I, II, and III segregation systems. Only the Type-II system uses actin-homologs during segregation, but all of these three systems utilize nucleotides hydrolysis in their segregation mechanism. This section gives a brief overview of these three systems.

TubZ (Type III) is a tubulin homolog found in *Bacillus thuringiensis* responsible for the segregation of the low copy number pBToxis (Aylett et al., 2010). TubZ utilizes GTP for its polymerization to form a parallel, double helical filament structure. After GTP hydrolysis, the filaments become weakened and depolymerizes (Aylett et al., 2010).

In *E. coli*, the ParA/SopA (Type I) proteins bind to the promoter region on low-copy-number plasmid to activate transcription of the par operon. This leads to the production of proteins ParA and ParB (Kenn Gerdes, 2000). ParA, in its ATP bound state, binds to the centromere-like site on the plasmid. Then ParB binds to ParA. This nucleoprotein complex at the centromere allows a Brownian Ratchet mechanism utilizing ATP to move the plasmid to opposite ends of a dividing cell. When the ATP is hydrolyzed, the nucleoprotein complex dissociates (Funnell, 2003).

The Type II system consists of a cytomotive filament that is an actin-homolog, an adaptor to bind DNA, and a centromere region on the plasmid. The addition of ATP drives filament assembly, providing the physical force to segregate plasmids (Jensen,

1997). The type II system is well characterized for the segregation of low copy number plasmid R1 in *E. coli* by the actin-homolog ParM (Fusinita van den Ent et al., 2002).

1.3 ParMRC Plasmid Segregation System

ParMRC is one of the well-characterized Type-II segregation systems. ParM has 12% amino acid identity to actin and was isolated from the low copy number plasmid R1 found in *E. coli* (Carballido-Lopez, 2006). The R1 is a multiple antibiotic resistant plasmid. (J. Møller-Jensen, Borch, J., Dam, M., Jensen, R.B., Roepstorff, P., and Gerdes, K. , 2003; Møller-Jensen, Jensen, Löwe, & Gerdes, 2002; J. Salje et al., 2010). In the ParMRC system, ParM is the cytomotive filament, ParR is the adaptor and parC is the centromere-like DNA region on the plasmid (Møller-Jensen et al., 2002).

1.3.1 Dynamic Behaviour of ParM

With the addition of ATP, ParM subunits assemble into filament (Fusinita van den Ent et al., 2002). Initially, ParM filaments are constantly polymerizing and depolymerizing to "search" for the adaptor protein ParR, which is bound to parC on the plasmid (E. C. Garner, Campbell, C.S., Weibel, D.B., and Mullins, R.D., 2007). Once the nucleoprotein complex is formed, ParM filaments segregate the plasmid by polymerizing bi-directionally (E. C. Garner, Campbell, C.S., and Mullins, R.D., 2004), physically pushing the plasmids to the opposite side of a dividing rod-shaped *E. coli* cell (C. S. Campbell & Mullins, 2007; J. Salje et al., 2010).

The behaviour which ParM filaments constantly polymerize and depolymerize to search for ParR-bound plasmids is known as dynamic instability (E. C. Garner, Campbell, C.S., and Mullins, R.D., 2004), and this mechanism is essential for plasmid

segregation (C. S. Campbell & Mullins, 2007). Dynamic instability in ParM occurs when ATP hydrolysis catches up to the growing filament end, where the ParM filament undergoes a conformational change to the "apo" state (Figure 1.3C), where the filament is destabilized and looks less compact (Fusinita van den Ent et al., 2002). ParM utilizes the capability to polymerize and depolymerize in order to search for parC bound ParR (J. Møller-Jensen, Ringgaard, S., Mercogliano, C.P., Gerdes, K., and Löwe, J., 2007). If ParM filaments cannot bind to a ParR-parC complex, the filament disassembles due to ATP hydrolysis, and allows the recycling of ParM subunits so they can polymerize in another direction to continue the search for ParR. On the other hand, it has been shown that nucleotide bound ParM filaments are more stable (E. C. Garner, Campbell, C.S., and Mullins, R.D. , 2004; J. Salje et al., 2010), and that the protofilament appears to be more rigid when stabilized (Figure 1.3C), because the protein domains moves to closes upon nucleotide binding (Fusinita van den Ent et al., 2002). In addition, ParM filament becomes stabilized when it binds to ParR, (J. Møller-Jensen, Ringgaard, S., Mercogliano, C.P., Gerdes, K., and Löwe, J., 2007) this is because ParR acts similar to an ATP cap in preventing filament disassembly. At this stage when the ParMRC nucleoprotein complex is formed, the ParM filament continues to assemble as more subunits are inserted at the contact site of ParM to ParR (J. Møller-Jensen, Borch, J., Dam, M., Jensen, R.B., Roepstorff, P., and Gerdes, K., 2003). ParM can be bound to ParR on both ends of the filaments, so the filament polymerizes bi-directionally and physically push the plasmids to the opposite ends of the dividing cell (J. Salje et al., 2010). However, new research suggests that ParR can bind ParM on only one end, not both, and the bundling is essential

for ParM bidirectional segregation (Bharat, Murshudov, Sachse, & Lowe, 2015; J. Salje, Zuber, B., and Löwe, J., 2009).

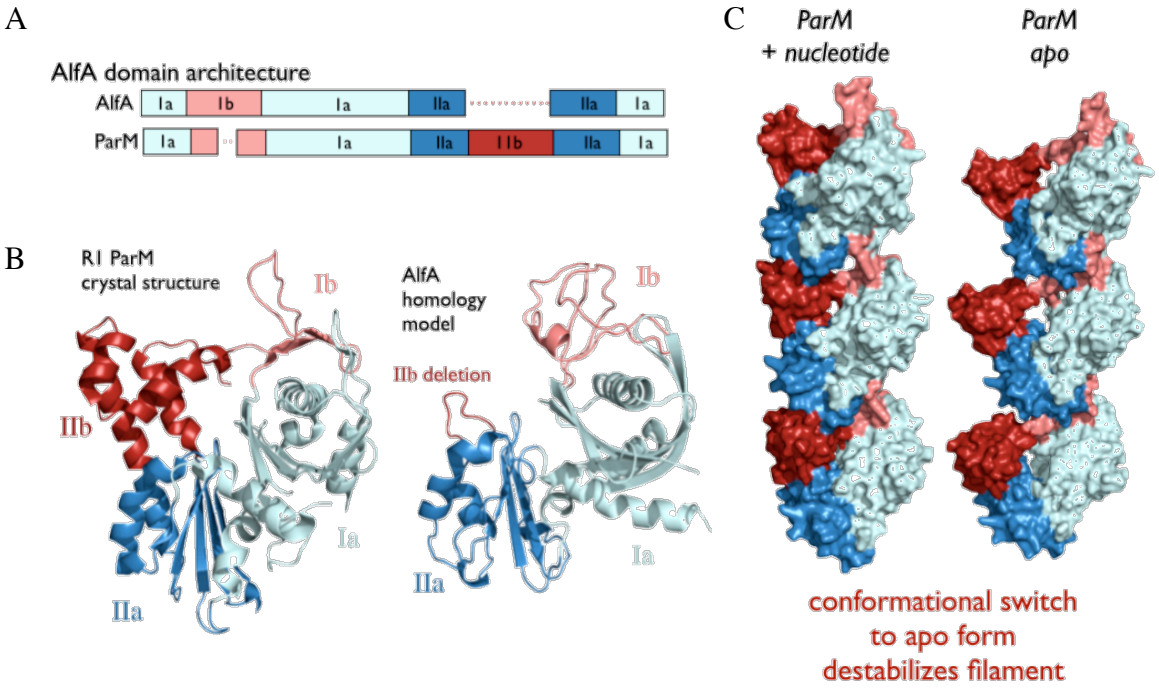

Figure 1.3 Comparison of AlfA to ParM. A) Alignment of AlfA and ParM sequences, exhibiting 15% sequence identity. B) Homology structure of AlfA constructed based on ParM R1 crystal structure, which shows that AlfA has a missing IIb domain. C) ParM is stabilized with the presence of ATP, but when the nucleotide is hydrolyzed the filament undergoes a conformational change to the *apo* form, which further leads to depolymerization if not capped by ParR.

1.3.2 Structure of ParM

ParM has been extensively studied by electron microscopy and X-ray crystallography (J. Salje, Zuber, B., and Löwe, J., 2009; Fusinita van den Ent et al., 2002). In its filament form, the ParM filament makes a left-handed helix with a 30^{o} twist (Galkin, Orlova, Rivera, Mullins, & Egelman, 2009). This is different from previously studied F-actin, which makes a right-handed helix and with a 27^{o} twist (Fujii et al., 2010). Nevertheless, the ParM subunit is composed of four domains that are similar to eukaryotic actin and prokaryotic actin subunits (Fig. 1.2). Figure 1.3B shows the

subdomain that the ParM crystal structure is composed of (clockwise from top): Ib, Ia, IIa, IIb. Figure 1.3B shows that there is an interdomain cleft between the IIb and IB, allowing the binding of nucleotides to this central pocket (Ozyamak, Kollman, & Komeili, 2013; Fusinita van den Ent et al., 2002). When the nucleotide is bound, the domains (I and II) moves ~25^{o} to close-off the interdomain cleft (Fusinita van den Ent et al., 2002), and resulting in a more rigid form allowing filament formation. This research on ParM helped to understand how the conserved actin core functions among eukaryotic and prokaryotic actins during polymerization. However, our preliminary research suggests that one prokaryotic actin, AlfA, does not possess the IIb domain (Figure 1.3A-B). This raises questions on how AlfA is capable of polymerization with an actin core different from previously seen in ParM (discussed in Section 1.4.1.1).

1.4 AlfA Segregation Complex

AlfA is encoded by and responsible for the segregation of pLS32 plasmids found in *Bacillus subtillis natto* (Tanaka, 2010). Like ParM, AlfA is a cytomotive filament responsible for pushing the plasmid during segregation. Accompanying AlfA, another protein AlfB is the adaptor that AlfA binds to. AlfB can bind to parN, which is a region on the plasmid DNA characterized by repetitive sequence for identification of AlfB binding. Interestingly, when AlfA is incubated with AlfB and ATP, the polymerization is inhibited and the critical concentration is increased, suggesting that AlfB alone inhibits AlfA. But when parN oligomers are added to the AlfA-AlfB mixture, polymerization will occur, suggesting that AlfB and parN could both regulate the assembly of AlfA *in vivo* (Polka, Kollman, & Mullins, 2014). AlfA segregate plasmid uni-directionally because

AlfA can polymerize only on one end. This is important for AlfA because it would ensure that new filament only grows from centromeric DNA (Polka et al., 2009).

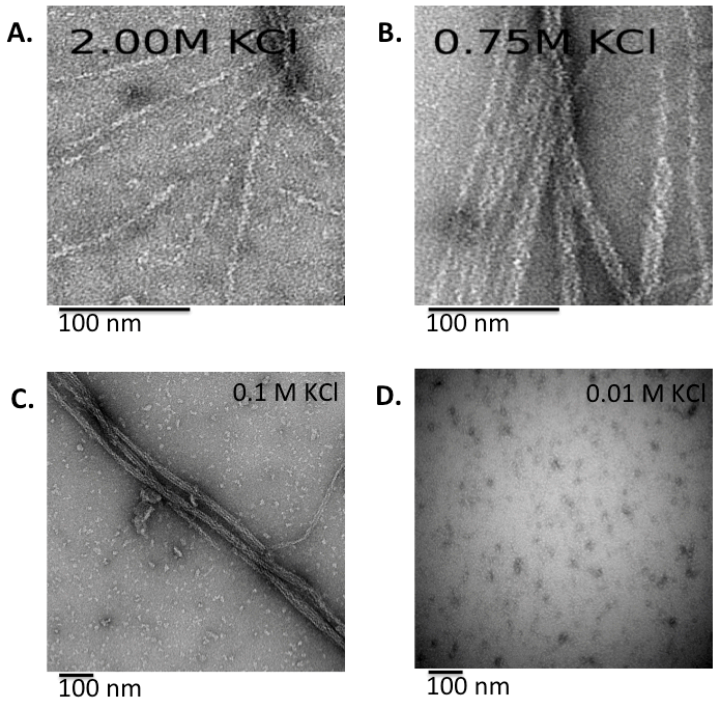

Figure 1.4 A-B: Adapted from (Polka et al., 2009). A: AlfA assembles into filament structures with 2.0 M KCl. B: AlfA bundles can be formed with decreasing salt. C: Negative stain TEM micrograph of WT AlfA assembled into a bundle structure at 0.1 M KCl (scale bar 100 nm). D: Negative stain TEM micrograph of WT AlfA in assembly buffer with 0.01 M KCl (scale bar 100 nm). The TEM micrographs were collected using a TF12 Microscope.

AlfA can readily assemble into bundles with the addition of ATP, ADP, and GTP (Figure 1.4C) and have a critical concentration of around 2.4 μM, 10 μM, and 2.0 μM respectively in 0.1 M KCl buffer (Polka et al., 2009). AlfA in higher salt concentration (e.g., 1.8 M KCl) effectively increases the critical concentration. In low salt such as 0.01 M KCl, AlfA will not assemble (Figure 1.4D). As the salt concentration gradually increase, the bundles can also breaks apart into filaments (Figure 1.4AB), suggesting that the bundles form as a result of electrostatic interactions (Polka et al., 2009). Bundling in biological conditions has not been seen in any other actins before, until recently ParM was seen forming bundles without crowding reagents (Bharat et al., 2015). Whether

bundling plays an important role in AlfA plasmid segregation is still unclear, because the functional significance of AlfA bundles during plasmid segregation has not yet been studied *in vivo*.

AlfA has different dynamic behaviour as compared to ParM. During a Total Internal Reflection Fluorescence (TIRF) microscopy experiment where fluorescence ParM was treated with ATP, fluorescence signals goes on and off constantly, suggesting continuous polymerization and depolymerization (Garner EC, 2004). However, TIRF microscopy of fluorescent AlfA treated with ATP shows persistent signals, suggesting that AlfA undergo polymerization but not depolymerization (Polka et al., 2009).

There is much significance for the research of AlfA. Bacterial plasmids can carry various genes beneficial for its survival, and some are harmful to human health. The study of AlfA as plasmid segregation mechanism may prove useful to design new drugs against pathogenic bacteria. The ability of AlfA to form well-ordered bundles also suggests the possibility of using AlfA as nanomachines for micromolecular forces, similar to Alp12 as an idea suggested by Popp et al. (2012). Lastly, because AlfA has partially conserved structure, similar longitudinal interactions and polymerization behaviors, a high resolution AlfA structure will better our understanding of F-actin and how it is evolved.

1.4.1 Structure of AlfA

To better understand AlfA, various techniques have been used to characterize its biochemical properties (as discussed earlier), but many questions still remain. A preliminary structure of AlfA filament has been reconstructed from data in high salt

negative stain TEM giving a resolution of 15Å (Polka et al., 2009). A higher resolution structure is required to gain understanding of why AlfA forms bundles and how the bundles function during plasmid segregation.

1.4.1.1 Homology Modeling

Secondary structure prediction and multiple sequence alignment of AlfA to hundreds of bacterial actin homologs revealed that AlfA shares structure similarities with ParM, in the arrangement of subdomains and left-handedness of filament. The multiple sequence alignment (Figure 1.3A) shows the domain architecture of AlfA to ParM. The Ib domain of AlfA is slightly larger than that of ParM due to longer sequence. However, AlfA is completely missing the IIb domain, which ParM and all other actins have. To further explore this mystery, a homology model was constructed based on the ParM crystal structure (Figure 1.3B). The homology model confirms that AlfA monomer is missing the IIb domain, which is at the site of nucleotide contact (Kollman Lab, unpublished data). The potential consequence of missing IIb domain in AlfA is unclear. In ParM, the IIb domain takes part in the conformational change from the closed state to the apo state. The IIb domain could play a role in the stabilization/destabilization of ParM and other actins. The question of how AlfA can form bundles and filaments without this IIb domain will be the basis for this research.

1.4.1.2 Cryo-EM Map

To improve the resolution of filament reconstruction, a mutant AlfA not capable of forming bundle was designed. This non-bundle forming mutant contains four charge-reversal mutations site, and is capable of forming only single filaments (Polka et al.,

2014). This mutant was purified using the ATP cycling method, and then assembled with ATP in 0.1 M KCl buffer, and lastly imaged using cryo-EM. Using the iterative helical real space reconstruction method, we obtained an electron density map of 7.5 Å resolution (Figure 1.5). Interestingly, the homology model can be docked neatly into the EM density map, which confirms that AlfA is missing IIb domain. However, the homology model is based on only 12% of ParM sequence, thus a high resolution crystal structure of the AlfA subunit is required to give more information on the nature of filament assembly contacts, and how the filaments form well-ordered bundles. This current cryo-EM structure (Figure 1.5), which the author of this paper helped to construct, is the basis of many functional studies carried out in this thesis.

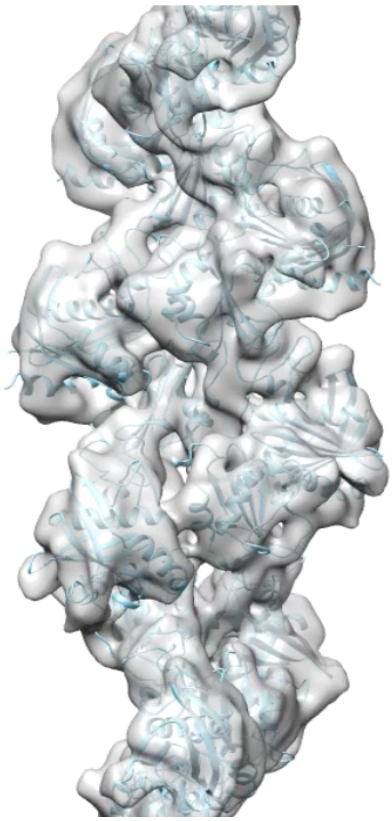

Figure 1.5. Cryo-TEM reconstruction with the homology model docked into the electron density map (7.5 Å). The reconstruction confirms that the missing IIb domain is a characteristic of AlfA filaments.

1.5 Research Objectives

It is unclear how AlfA filaments are held together. Based on previous research, AlfA bundle breaks apart as the KCl concentration gradually increases, so we hypothesize that AlfA filaments form due to electrostatic interactions. Based on this hypothesis, non-assembling mutants will be designed by reversing the charge of certain residues at the filament assembly interface. A successful non-assembling mutant will not form filaments. In this research, we have generated, purified, and identified non-assembling mutants for understanding the filament contact sites (Fig. 4.1).

It is unclear how AlfA filaments compensate for this missing IIb domain. The multiple sequence alignment was a surprising result, because in all available actin filament the IIb domain is involved in the longitudinal contact between each protofilament. To solve this mystery, AlfA will be crystallized and docked into the cryo-EM map to generate a pseudo-atomic model. AlfA non-assembling mutants will also be used in the crystallization trials, because the previous crystallization attempts for actins were unsuccessful. Initial screens done by Dr. Justin Kollman using wild-type AlfA did not produce any crystals. This could be due to the highly dynamic unstructured regions in filament, thus decreasing the chances of forming a single population of protein crystals. This was previously seen in TubZ (Aylett et al., 2010), when a truncated filament free of unstructured regions was successfully crystallized. We hypothesize that the missing IIb domain is what gave rise to AlfA's unique dynamic behaviour and bundle structure. In this research, truncation constructs free of unstructured regions were generated based on secondary structure prediction and mass spectrometry results, but these truncated protein

did not produced any crystals. However, we have reproduced protein crystals not capable for diffraction using wild-type AlfA, which was contrary to initial expectation (Fig. 5.1).

It would also be interesting to examine the functional importance of AlfA polymerization *in vivo*, and the consequence of losing AlfA during plasmid segregation. We hypothesize that AlfA polymerization and bundle formation is critical for plasmid segregation. We will introduce non-filament forming mutants or non-bundling mutants into plasmids, and plasmids with truncated AlfA to test the consequences of losing AlfA filaments during segregation. It would be expected those plasmids, which were truncated, and plasmids which contain mutations to produce non-assembling AlfA would have a plasmid loss rate higher than that of the wild-type plasmids. The wild-type plasmids would have a small loss rate, because plasmids cause metabolic stress on the cell so they are likely to be discarded by some bacteria (Becker E, 2006). In this research, we found that pBET131 plasmids with truncated AlfA have significantly higher loss rate than that of wild-type plasmids (Fig. 4.2), and confirming our hypothesis.

Additionally, purified AlfA from previous works in our lab exhibit a doublet pattern when run on SDS-PAGE. Since most bacteria do not have post-translational modification mechanisms, it is unclear if AlfA was degraded or cleaved during purification. To obtain pure AlfA for crystallization trials, we will examine the composition of the upper and lower band seen on SDS-PAGE by using mass spectrometry. We hypothesize that the upper band is the full-length and the lower band (which runs faster) is the degraded product. Our results contradict the hypothesis, where the data suggests that the lower band is actually the full-length protein (Fig. 3.3, 3.4, 3.5).

Chapter 2- Material and Methods

2.1 Particle Picking

From cryo-EM micrographs obtained using the Krios, particles were boxed using the EMAN1.9 software (Polka et al., 2009) with a box size of 10 units, Overlap of 4 units and A/Fix of 4.4 units. A total of two million particles were boxed. The reconstructed density maps had the homology model docked in, and was visualized with Chimera (Pettersen et al., 2004).

2.2 Mass Spectrometry (MS)

Wild-type AlfA fractions from MonoQ were collected and ran on SDS-PAGE with 1 mm BME, stained with Coomassie Blue G-250 and then destained with 10% methanol, 5% glacial acetic acid, and 85% dH_2O. The lanes that showed clear upper and lower bands of AlfA were kept, and re-ran on SDS-PAGE. After Coomassie destain, the bands were carefully excised from the gel under a strong ultraviolet lamp, and then sent for tryptic digestion MS at IRCM and INRS. The INRS facility was not provided with information about the protein, so the MS results were matched to protein using BLAST.

2.3 Subcloning and PCR

2.3.1 Optimized AlfA

An optimized AlfA DNA sequence with optimized codon usage in *E. coli* were synthesized and cloned into pBET-20b(+) vector between the restriction sites BamHI and NotI (Polka et al., 2009). This vector contains the T7 promoter.

2.3.2 Subcloning into pSMT3

The AlfA was inserted into a new vector for better purification approaches. First, the AlfA containing pBET-20b(+) vector was amplified using PCR with forward and reverse primers, and then digested with restriction enzymes (BamHI and NotI). The product was then purified using a PCR clean-up kit (Qiagen®).

The new vector was pSMT7 obtained from Dr. Bhushan Nagar. The pSMT3 vector have a *lac* operon, a T7 promotor, and a multiple coloning site containing the restriction sites BamHI and NotI. The pSMT3 also contain six histidine tag and a SUMO tag three codon before the multiple cloning site (Lima, 2009). To prepare the open vector, the vector was treated with restriction enzymes BamHI and NotI, and then treated with calf intestinal phosphatase to produce an open vector with no free 5' phosphate. The product is then run on agarose gel and purified by gel clean-up kit (Qiagen). The open vector and insert was ligated overnight and then the product of ligation was transformed into TOP10 competent *E. coli* cells.

2.3.3 Transformation

To transform DNA into $RbCl_2$-treated competent cells, DNA is incubated with cells on ice for 30 minutes, heat-shocked for 40 seconds at 42^{o}C, grown in liquid LB at 37^{o}C for one hour, and then plated on selective media (McManus, 2013).

2.3.4 DNA Extraction, Sequencing and Colony PCR

Plasmid DNA was extracted using Geneaid® Miniprep Kit with the following steps: lysis, neutralization, binding to membrane, wash and then elution. The DNA

elution product was checked for purity using a Nanodrop spectrophotometer, and then sent for Sanger sequencing at Genome Quebec (Nanuq, 2013).

To ensure that AlfA was cloned successfully into the vector, colony PCR were done as an extra step. For each PCR, TOP10 cell colonies were inoculated into PCR reaction tubes as the template. Then the PCR products were run on agarose gel to check for amplification.

2.3.5 Site Directed Mutagenesis

Site directed mutagenesis were used to generate AlfA mutants. All of the non-assembly mutants and truncation constructs were generated using the 3'-overhang primers. The Agilent and NEB design primers were also used in site-directed mutagenesis reactions of pBET131 plasmid.

2.3.5.1 The 3'-Overhang Primers

These forward and reverse primers contain: the site of mutation, one or more C/G at 5' and 3' end, an overhang at the 3' end of at least 8 nucleotides, and mutation content of less than 17.5% (Zheng, Baumann, & Reymond, 2004). PCR were then performed with these primers, and the product digested with Dpn1, transformed into TOP10 competent cells, have DNA purified by miniprep, and then sequenced the DNA at Genome Quebec. For detailed protocol please see Zheng et al., 2004. The polymerases used were *iPfu* and *Phusion* from NEB.

2.3.5.2 The Agilent Complete Overlap Primers

These primers are used with the Quickchange® protocols. The forward and reverse primers contain: the site of mutation, one or more C/G at 5' and 3' end, balanced G/C and A/T content and mutation content of less than 10%, and a high melting temperature of 78°C. The forward and reverse primers completely overlap one another. The PCR were done in a similar steps to 2.3.5.1 (Agilent, 2013). The *iPfuTurbo polymerase* (from Agilent) and *Phusion polymerase* (from NEB) were used in these PCR reactions.

2.3.5.3 The NEB Non-Complementary Primers

The forward and reverse primers are designed back-to-back, where the forward primer contains the site of mutation, but the reverse primer bind to the complementary template in opposite direction to the forward primer. These primers have balanced GC/AT contents and melting temperatures of no more than 72°C. The PCR amplification generates linear double stranded DNA, so they were treated with T4 polynucleotide kinase, ligase, and then Dpn1. The products were transformed into TOP10 competent cells, have DNA purified by miniprep, and then sequenced the DNA at Genome Quebec. The *Phusion polymerase* and *Phusion Hot Start polymerase* from NEB were used for these PCR reactions (NEB, 2015).

2.3.6 Truncating AlfA in pBET131

A part of the AlfA sequenced was excised from pBET131 (Teruo Tanaka, 1998), so the new plasmid was used as a negative control for the plasmid loss assay. This was done using the restriction enzymes SacI and SnaBI from NEB. After the digestion, the

products were run on agarose gel, excised, and then purified. The purified DNA was then treated with Klenow® fragment remover and ligated overnight. Lastly, the ligation product was transformed into TOP10 cells. Using a miniprep (Geneaid®) kit, the DNA was extracted, sent for sequencing, and then transformed into competent *Bacillus subtilis* PY79 cells.

2.4 Protein Expression

2.4.1 Transformation and Test Induction

The successfully sequenced DNA was transformed into BL21 (DE3), BL21 (pLYSS), and C43 competent cells. Colonies were picked the next day from the antibiotic plate, grown in 10 mL LB overnight. On the next day a fresh culture of LB was incubated, grown to OD_{600} of 0.8 and induced with IPTG at 37^{o}C for 2 hours. The cells were centrifuged, lysed by sonication and ran on SDS-PAGE to check for test induction of AlfA protein (Polka et al., 2009).

2.4.2 Large Scale Induction

Glycerol stocks were prepared by adding 600 μL of cell culture into 600 μL of sterile 50% glycerol, and then frozen at 80^{o}C. From glycerol stocks, 10mL LB was inoculated and grown overnight, and then 1L culture was inoculated and grown to OD_{600} of 0.8~1.0, and then cooled down to 20^{o}C, and then induced with IPTG overnight at 20^{o}C. The cell pellets were harvested for protein preparation by centrifugation (Polka et al., 2009).

2.4.3 SDS-PAGE

The SDS-PAGE gels were cast using the protocol provided by BioRad. Gels were loaded using sample buffer mixed with protein, and ran with voltages 110-200 V for 40-90 minutes. The gel was then stained with Coomassie Blue G-250 and then destained with Kimwipes®.

2.5 Protein Purification

Initially, the cell pellet was thawed on ice, lysed with the presence of 1 mM PMSF, and pelleted by centrifugation. For further purification, the supernatant (cell lysate) can be loaded on FPLC or ATP cycled (explained in 2.5.1).

2.5.1 Purification by ATP Cycling and Pelleting Assays

AlfA from pBET-20b(+) or pSMT3 were lysed, precipitated using ammonium sulphate, and then resuspended in polymerization buffer. The AlfA polymers were subjected to ultracentrifugation. The pellet fraction is treated with EDTA for disassembly and then dialyzed into assembly buffer. The dialyzed products were purified by ATP assembly and EDTA disassembly for additional two times (Polka et al., 2009).

Pelleting assays were carried out in a similar method. The AlfA protein was initially cleared of aggregation by ultracentrifugation. Then the supernatant fraction was polymerized in assembly buffer (0.05 M Tris-HCl pH 7.5, 0.1 M KCl, 10 μM ATP, 10 μM $MgCl_2$) for 10 minutes at room temperature, and then centrifuged at 80,000 RPM. The supernatant and pellet fraction were analyzed on SDS-PAGE (Polka et al., 2009).

2.5.2 Purification Methods

FPLC purification methods were used for AlfA expressed using the pSMT3 vector. The pSMT3 vector contains one SUMO tag, and six poly-histidine tags allowing binding to Ni^{+}NTA (HisTrap® column or Ni^{+}NTA Agarose MCLAB). The cell was lysed, loaded onto Ni^{+}NTA, and then eluted with imidazole. The eluted fractions were combined, dialyzed in buffer without imidazole in SnakeSkin® Tubing (10 kD cut off), and then cleaved with ubiquitin like protease 1 (ULP1) which effectively cuts off the His-SUMO tags. The cleaved protein was loaded onto Ni^{+}NTA again, with the flow-through fractions collected and then concentrated using Amicon Ultracel® (10 kD cut-off). At this point the protein was ready for anion exchange (HiTrap® column or MonoQ® column), and then size-exclusion chromatography (or gel filtration using Superdex200® columns). Please refer to Figure 2.1 for a full illustration of FPLC purification of AlfA (Lima, 2009; Polka et al., 2009).

2.5.2.1 Ni^{+}NTA Column

Protein was allowed to bind with Ni^{+}NTA resin for one hour in non-reducing buffer (50 mM Tris-HCl pH 7.5, 100 mM KCl, 10 mM imidazole, 1 mM PMSF) with minimal stirring. The resin was then washed with a high salt buffer (50 mM Tris-HCl pH 7.5, 500 mM KCl) and then a low salt buffer (50 mM Tris-HCl pH 7.5, 10 mM KCl). Then the protein was eluted with 200 mM to 500 mM imidazole. In the first Ni^{+}NTA experiment the imidazole elution contains AlfA, but in the second Ni^{+}NTA experiment the flow-through and washes contain AlfA. This flow-through was loaded onto the anion exchange chromatography.

2.5.2.2 Anion Exchange Chromatography

The column was washed with low salt buffer (50 mM Tris-HCl pH 7.5, 10 mM KCl). The flow-through from the second Ni^{+}NTA was concentrated and then diluted using 50 mM Tris-HCl buffer to low salt (10 mM KCl), and then loaded onto the column. For HiTrap columns, the protein was eluded with a linear gradient of salt. MonoQ® column was used to obtain samples of higher purity for crystallography, and the protein was eluded with an optimized stepped gradient. Fractions were collected and ran on SDS-PAGE before size-exclusion chromatography.

2.5.2.3 Size-Exclusion Chromatography

The anion exchange fractions were combined and then concentrated to less than 5% of the total HiTrap column volume. The void volume was disgarded, and then the fractions were collected, concentrated using Amicon Ultracel® (10 kD cut-off), ran on SDS-PAGE, and then concentrated for TEM or X-ray crystallography.

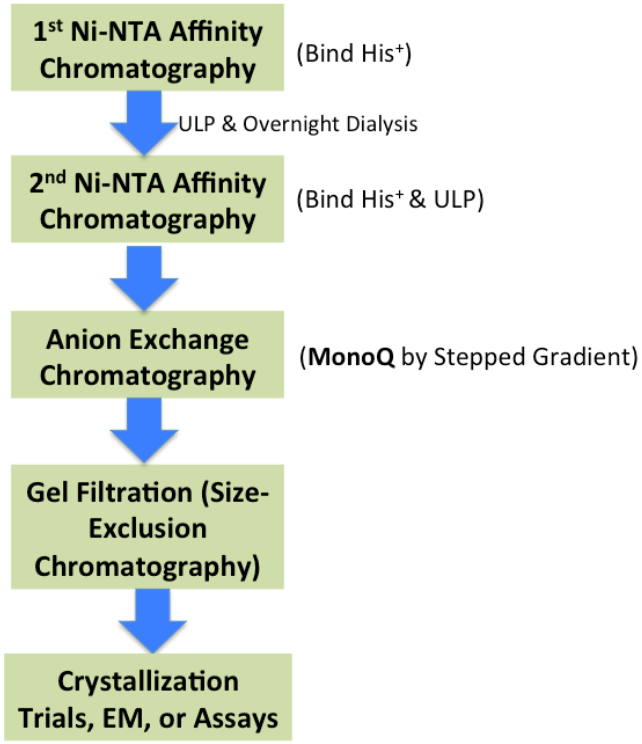

Figure 2.1 Illustration of the AlfA purification by FPLC methods.

2.6 Negative Staining TEM

Carbon films on mica sheets were obtained from Facility of Electron Microscopy Research at McGill University, Montréal, Québec. The copper grids obtained from Electron Microscopy Science were coated with carbon. These carbon coated copper grids were then glow discharged. Proteins were thawed on ice and then ultracentrifuged to pellet aggregates. Then AlfA in assembly buffer was loaded onto the copper grids. The protein was blotted by filter paper followed by three washes with double distilled water and then staining with uranyl formate three times (Polka et al., 2009). Then the stain was blotted and the grid was examined using the T12 microscope, and then pictures taken using the TF20 microscope at FEMR, McGill University. The T12 setups are: an acceleration voltage of 120 keV, magnification of 52,000X with CCD detector. The T20 setups are: an acceleration voltage of 200 keV, magnification of 68,000X with CCD detector.

2.7 Crystallization Screening

2.7.1 The 96-well Plates and Initial Screening

Purified proteins (or protein reactions) were initially set up with NeXtal screens by Pheonix Robot in 96 well plates for screening. The drops are in wells next to the reservoir (sitting drop method). The plates were then stored at 22^{o}C or 4^{o}C. The wells were screened manually under dissection light microscopies that have birefringence lens. Plausible hits were examined under the UV microscope. Big crystals were shot directly

with an X-ray source (with or without cryo-protectant). Small crystals were made larger by being reproduced in 24-well plates.

2.7.2 The 24-well Plates and Optimization

Purified proteins (or protein reactions) were set up manually into 24-well plates, with bigger drop sizes (1-2 μL). The drops were set on coverslips over the reservoir (hanging drop method). To optimize the hit and encourage better crystals, different crystallography variables were changed around the hit conditions, such as pH, buffer typessup, temperature, reducing agents, nucleotides, protein concentrations, glycerol content in the protein reactions and reservoirs.

2.7.3 The Additive Screens

Additive screens containing different hydrophilic (e.g., salts) or hydrophobic (e.g., polyethylene glycol) compounds were added to the optimized crystal hit by Pheonix Robot in 96-well plates. The conditions could be further optimized in 24-well plates.

2.8 **Plasmid Loss Assay**

Generation time of PY79 *Bacillus subtilis* cells were determined by growing the cells in liquid LB (with and without antibiotic) at 20^{o}C, 30^{o}C and 37^{o}C and measuring the OD_{600} once every hour.

Overnight cultures of PY79 *Bacillus subtilis* cells from liquid LB containing antibiotic (10 μg/mL tetracycline) were inoculated into fresh LB without antibiotics. Then the cultures were diluted to OD_{600} of 0.2 for every generation time passed. The cells were grown for 10, 20, or 30 generations, and then plated onto non-selective medium.

Isolated colonies were picked and streaked onto selective medium (10 μg/mL tetracycline) to score for the loss of the plasmid-associated drug resistance (Becker E, 2006; Polka et al., 2014; Tanaka, 2010). See Figure 2.2 for a detailed illustration of the protocol. The plasmid loss rate per generation was determined by:

Equation 2.1 $$r_{final}=r_2e^{-(1-L)g}$$ (Polka et al., 2014)

Where r_{final} is the final fraction of resistant colony count, r_2 is the fraction of resistant colony count at second generation (overnight culture being the first generation), g is the number of generations passes, and L is the loss rate per generation.

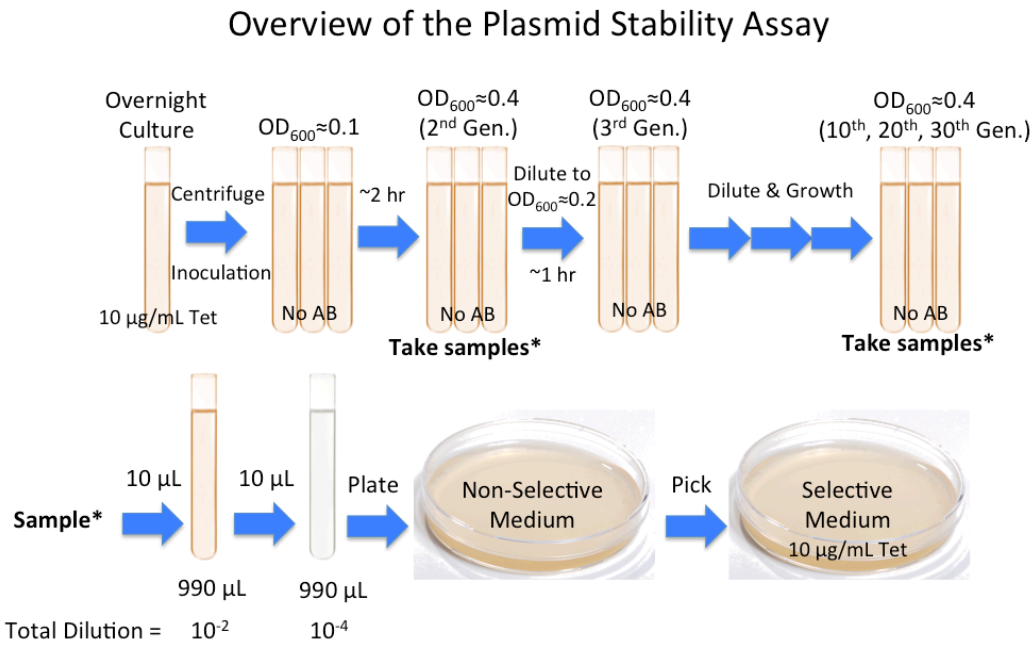

Figure 2.2 Overview of the plasmid loss assay (or plasmid stability assay) in a detailed overview.

2.9 Making Chemically Competent Cells

The *E. coli* competent cells (BL21 DE3, C43, TOP10, DH5α, MG1655 strains) were prepared by resuspending the cell pellets in solution containing $RuCl_2$ and $CaCl_2$ for creating "membrane pores" during heat shock transformation (McManus, 2013).

However, the *Bacillus subtilis* PY79 competent cells cannot be prepared by this technique. Instead, the PY79 cells were grown in minimal media for starvation, and were resuspended in solution containing $CaCl_2$ and $MgCl_2$. To transform, the PY79 competent cells were incubated with DNA and grown in minimal media to activate sporulation mechanisms for DNA uptake (Cambridge, 2008; Stephens, 1998).

Chapter 3: AlfA Subcloning, Expression, and Purification

3.1 Introduction

Purified AlfA bundles and filament assembly has been reconstituted *in vitro* (Polka et al., 2009), however it is unclear of how filaments are held together, and what residues are responsible for this action. Previous research suggests that AlfA filament form as a result of electrostatic interactions (Polka et al., 2009), therefore it may be possible to generate AlfA not capable of polymerization by mutating certain charged residues on the barbed end, pointed end, or cross-stranded interface. If these charge-reversal mutations could produce polymerization incompetent AlfA, then it is possible to learn what residue is responsible for holding the filament structure together.

Previously, AlfA were purified by ATP cycling based on the polymerization property of AlfA. Polymerization incompetent mutants cannot assemble into filaments, so if they were to be purified, a new protocol would be required. Thus, a new purification protocol was created to purify both polymerizing and polymerization incompetent AlfA.

The pSMT3 plasmid has the His-SUMO (small ubiquitin like modifier) tag three codon before the multiple cloning sites. Consequently, the translated protein would contain six histidine residues followed by SUMO at the N-terminus of the fusion protein. The SUMO and the start of AlfA protein would be separated by one serine residue. The histidines allow binding to Ni^{+}NTA, and the SUMO can be released by treatment with the protease ULP1 (ubiquitin like protease 1). Note that the ULP1 also has a polyhistidine tag. The first Ni^{+}NTA binding allows other proteins in the lysate to be discarded. Then

ULP1 cleaves off at the SUMO tag, leaving AlfA protein that cannot bind to a second Ni^{+}NTA run. This is further purified on FPLC as described in Chapter 2.

3.2 Wild-type Purification by FPLC

After AlfA was successfully subcloned into the pSMT3 plasmid (as suggested by sequencing results and colony PCR), the wild-type AlfA was used to optimize FPLC purification. Initially AlfA expression was test induced with iPTG and the colony with the greatest protein expression was used for large-scale induction. To optimize induction, the duration and temperatures of induction were also tested. BL21 (DE3) cells have a lower protein yield than C43 cells (results not shown). Figure 3.1A shows the purification steps of AlfA from lysis to elutions during the first Ni^{+}NTA chromatography, ULP1 cleavage, and second Ni^{+}NTA chromatography. During the dialysis and ULP1 cleavage, the protein precipitates in low salt buffer (0.1M KCl). So the protein was centrifuged to separate into the pellet and supernatant fractions. The supernatant fraction was used for the second Ni^{+}NTA, which gave a relatively clean product that can be FPLC purified.

Figure 3.1B shows that the AlfA starts to elute at a conductivity of 20 mS/cm, which corresponds to a KCl concentration of 200 mM. At the peak volume 90 mL, the conductivity was 35 mS/cm. The fractions from this peak was combined and loaded onto the Superdex S200 column for gel filtration (size-exclusion chromatography), shown in Figure 3.1C. In this elution profile, AlfA eluted as a single peak. When ran on 12% SDS-PAGE (Fig. 3.1D), the sample had a light upper band and a strong lower band. When the protein was treated with ATP and $MgCl_2$, it readily assembles into bundles (Figure 3.1E).

However, at this point it was unclear about the composition of the upper and lower band.

It was later discovered that increasing the KCl concentration in the purification buffers to 0.5 M would increase the solubility of wild-type and mutant proteins in solution. Wild-type AlfA that was insolubilized in low salt buffer could be "rescued and re-solubilized" by adding KCl to 0.5 M, and had the ability to assemble into bundles.

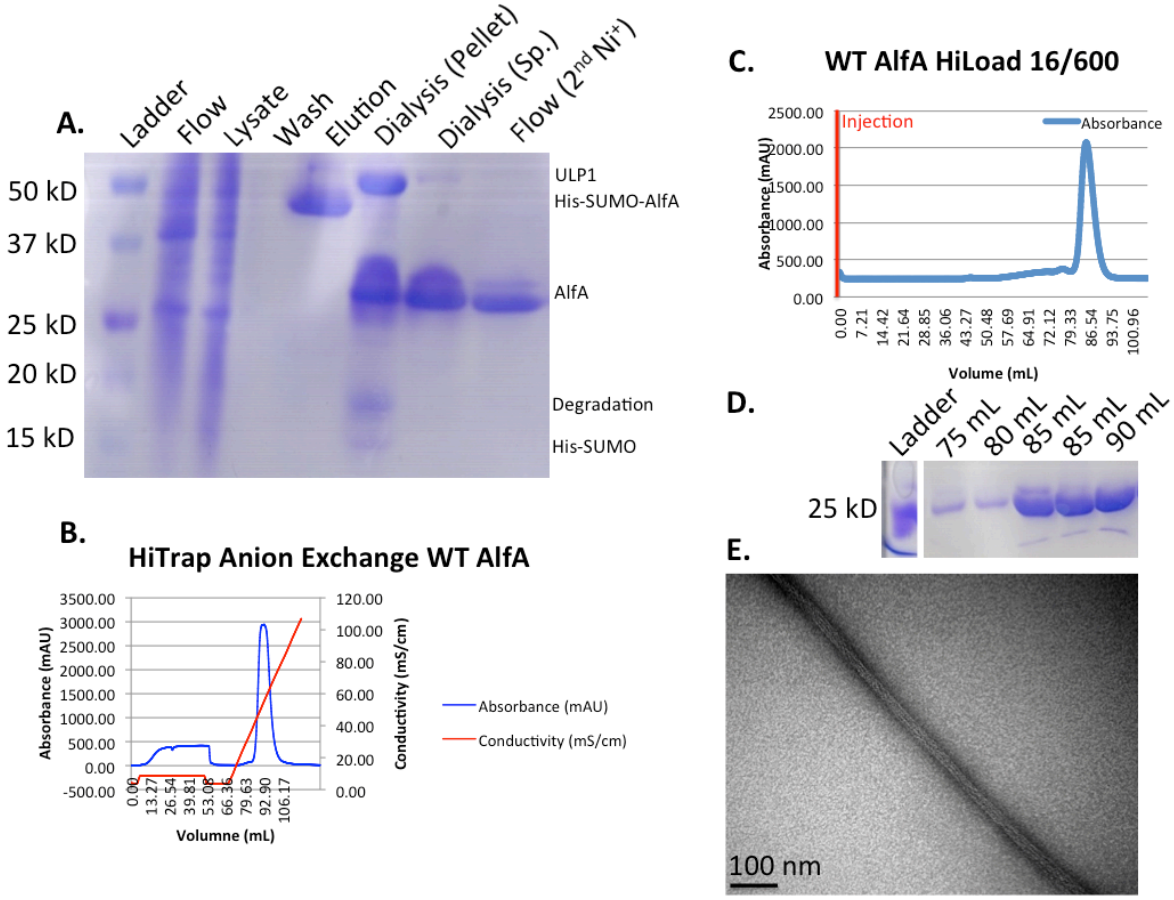

Figure 3.1. A: Purification of wild-type (WT) AlfA with protein fractions ran on SDS-PAGE under reducing conditions (1 µM BME). B: HiTrap anion exchange purification of WT AlfA using the desalted 2nd Ni^{+}NTA flow through. The UV absorbance is the baby blue curve measured in mAU and the conductivity is the red curve measured in mS/cm, where 10 mS/cm is approximately 100 mM KCl. C: Purification of WT AlfA using the HiLoad 16/600 gel filtration column, using the HiTrap anion exchange products. The column volume is 124 mL, the red vertical line indicate the point of protein injection, and the dark blue curve indicates the UV absorbance. D: The fractions of the HiLoad 16/600 fractions ran on SDS-PAGE under reducing conditions (1 µM BME). E: Negative stain TEM micrograph of WT AlfA (HiLoad fractions) assembled into a bundle structure (scale bar 100nm). The TEM micrograph was collected using TF20 Microscope.

3.3 Modification to Protocol to Separate Proteolytic Fragment

MonoQ is a type of quaternary ammonium anion exchange resin that has higher resolution than the HiTrap Sepharose anion exchange resin. The elution profile using the MonoQ column produced two overlapping peaks. To separate these two peaks into homogeneous peaks, the MonoQ run was optimized to perform stepped gradient on increments of 50 mm KCL. As can be seen in Figure 3.2A, the elution profile of anion exchange using the MonoQ column (stepped gradient) appears very different from HiTrap column (Figure 3.1B). The MonoQ column produces several peaks, whereas the HiTrap column produced only one homogeneous peak. The fractions under the peak were collected and then combined. Then these fractions were ran ran on 12% SDS-PAGE, the AlfA upper and lower bands were separated for the first time, as previous purification using ATP cycling or FPLC were not able to separate the upper band from the lower band. Figure 3.2B suggests that Fractions B is a homogeneous solution of the lower band, whereas Fractions D contains a dominant solution of the upper band. Fractions C is somewhere in between, containing twice as much lower band as the top band, similar to previous purifications.

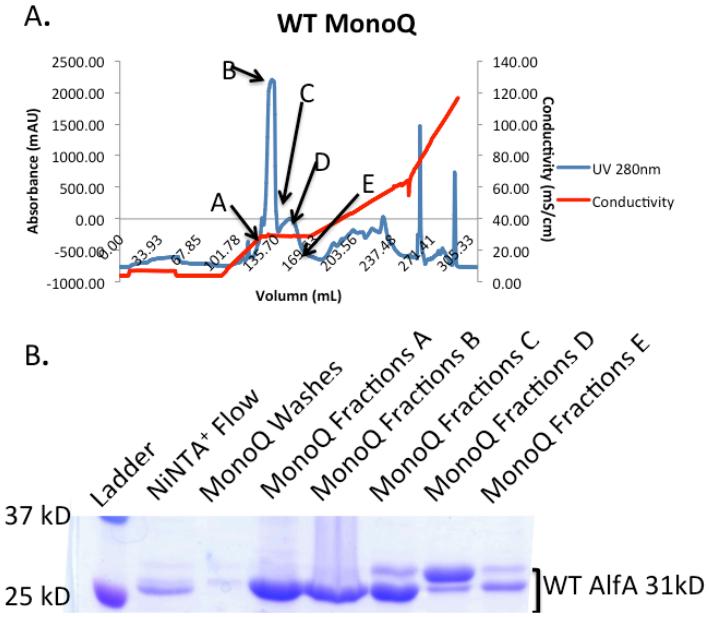

Figure 3.2. A: Wild-type AlfA purification using the Mono Q 10/100 GL column, with labeled peaks (from left to right) in ascending alphabets. The dark blue line indicates the UV absorbance measured in mAU, and the red line indicates the conductivity values measured in mS/cm, where 10 mS/cm approximates to 100 mM KCl. B: Fractions from the same MonoQ run on SDS-PAGE under reducing conditions (1 µM BME), with fractions corresponding to the labeled peaks in A.

The upper and lower band fractions were loaded onto Superdex S200 for gel filtration chromatography. Bottom band fractions from MonoQ were loaded onto the 10/300GL column, giving two main peaks (Fig. 3.3A). When ran on SDS-PAGE (Fig. 3.3B), the first peak and the shoulder that follows (9-14 mL) contained a very small amount of upper band AlfA. The rest of the second peak appears to be a homogeneous solution of lower band AlfA (15-20 mL). Additinally, when the upper band fractions from MonoQ were loaded onto the 24 mL volume 10/300GL column, it produced two overlapping peaks again. So it was further purified using the HiLoad 16/600 column that would have a higher resolution (Fig. 3.3C). The HiLoad 16/600 column produced three peaks. The third peak on Figure 3.3B eluted at around the same volume as previously

purified doublet AlfA (Fig. 3.1C). When all three peaks were examined on SDS-PAGE, all the fractions had doublet AlfA (Fig. 3.3D).

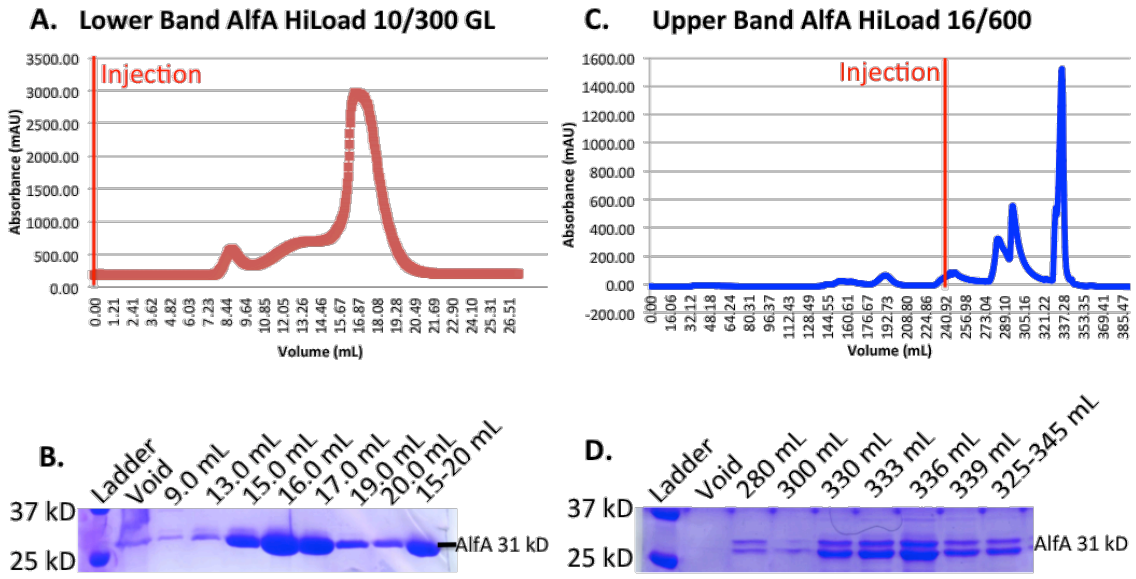

Figure 3.3. A: Purification of wild-type (WT) lower band AlfA fractions from MonoQ using HiLoad 10/300GL gel filtration column. The column volume is 24 mL, the red vertical line indicates the point of protein injection, and the orange curve indicates the UV absorbance of AlfA measured in mAU. B: The fractions of A loaded onto SDS-PAGE under reducing condition (1 µM BME), with volumes corresponding to the volumes on the chromatograph. C: The purification of WT AlfA using HiLoad 16/600 with upper band fractions from a second MonoQ run followed by a HiLoad 10/300GL. The column volume is 124 mL, the red vertical line indicates the point of protein injection, and the blue curve corresponds to the UV absorbance of AlfA in mAU. D: The fractions of C loaded onto SDS-PAGE under reduding conditions (1 µM BME). The doublet pattern persisted.

3.4 Identifying Proteolytic Fragment by Mass Spectrometry

It was presumed that the upper band is the full-length protein and the lower band was a degradation product, so assembly reactions were done for both purified proteins and then visualized using negative staining TEM. However, under negative staining TEM, the bottom band fractions assembled into filaments and bundles (Fig. 3.4A) but the upper band fractions did not assemble (Fig. 3.4B). To confirm this result, mass

spectrometry was done to analyze the composition of proteins in the upper and lower bands using SDS-PAGE bands from Figure 3.2B.

A.

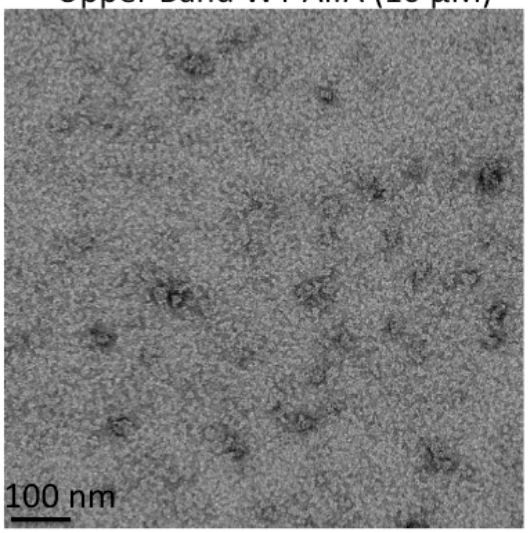

B.

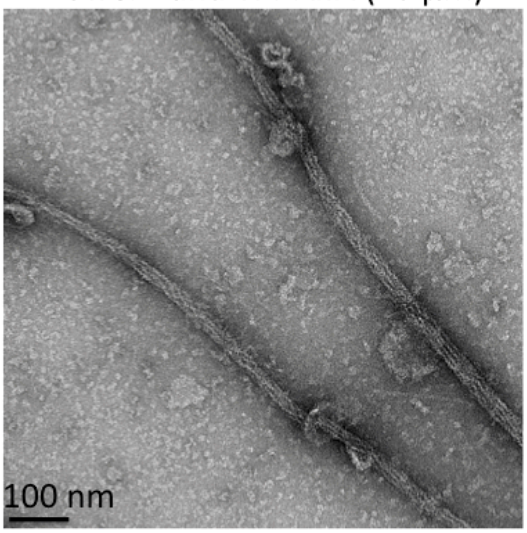

C.

Protein N-term peptide	Intensity 4% Injection			Intensity 0.2% Injection		
	Lower	Upper	Difference L/U	Lower	Upper	Difference L/U
(-)mTLTTVIDIGNFSTK(Y)	3.34E+06	3.17E+06	1.05	3.77E+04	15000	2.51

D.

Protein C-term peptide	Intensity 4% Injection			Intensity 0.2% Injection		
	Lower	Upper	Difference L/U	Lower	Upper	Difference L/U
(R)KFEEmFA(-)	2.77E+08	3.67E+06	75.48	3.10E+07	5.70E+05	54.39
(K)FEEmFA(-)	3.45E+06	2.85E+04	121.05	2.17E+05	1.90E+03	114.21

Fig 3.4. A: Negative stain TEM micrograph of WT AlfA (HiLoad 10/300GL upper band fractions) in assembly buffer (scale bar 100 nm). B: Negative stain TEM micrograph of WT AlfA (HiLoad 16/600GL lower band fractions) in assembly buffer (scale bar 100 nm). The TEM micrographs were collected using TF20 Microscope. C: Mass spectrometry analysis of the intensity of N-terminal peptide, showing little different in intensity between lower and upper bands. D: Mass spectrometry analysis of the intensity of C-terminal peptides, showing significant difference in intensity between lower and upper bands.

Results from two different mass spectrometry facilities (IRCM and INRS) suggested that the upper band from SDS-PAGE was a degradation product, whereas the lower band was a full-length protein. Figure 3.4C and 3.4D are analysis of peptide intensity from IRCM. In Fig. 3.4C, the intensity of N-terminal peptide

mTLTTVIDIGNFSTK(Y) from both lower and upper bands were analyzed. With 4% injection of trypsin-digested samples, it was found that this peptide had a similar intensity/abundance in both upper and lower band. With 0.2% injection of trypsin-digested samples, it was found that this peptide had a slightly higher intensity/abundance in lower band than in upper band. In Fig 3.4D, the intensity of C-terminal peptides (R)KFEEmFA and (K)FEEmFA from both lower than upper bands were also analyzed. It was found that with 4% sample injection, both of these peptides had significantly higher intensity in the lower band than in the upper band. With lower percentage injection (0.2%), the intensity of these peptides remains to be significantly higher in the lower band than in the upper band.

3.5 Designing, Expressing, and Purifying the Truncation Constructs

After learning the mass spectrometry results and its interpretations, AlfA truncation constructs were designed and then purified for EM and crystallography. Secondary structure prediction (PSIPRED) shows that R268/K269 could be part of a random coil between two alpha helixes. In conjunction with the mass spectrometry results, a truncation construct was designed by inserting a stop codon as R268/STOP/K269 (ΔK269). Alternatively, another secondary structure prediction done two years ago using a different algorithm showed that K265/Y266 could be part of a random coil. So another truncation construct was designed by inserting two stop codons as K265/STOP/STOP/Y266 (ΔY266). Both constructs were sub-cloned, expressed, and purified in wild-type AlfA and polymerization incompetent mutants.

In wild-type AlfA truncation constructs, the second Ni^{+}NTA flow through did not exhibit the doublet pattern on SDS-PAGE (Figure 3.5A-B). To verify this phenomenon, the Ni^{+}NTA flow through was loaded onto the MonoQ column, and produced a single peak, with a similar elution profile as previously seen in Figure 3.1B. The fractions from MonoQ column were further analyzed on SDS-PAGE, and only one AlfA band was present. When the MonoQ fraction, which was later purified by gel filtration for crystallography was run side-by-side with wild-type AlfA, it was observed that the truncation construct contained the lower band AlfA (Figure 3.5C).

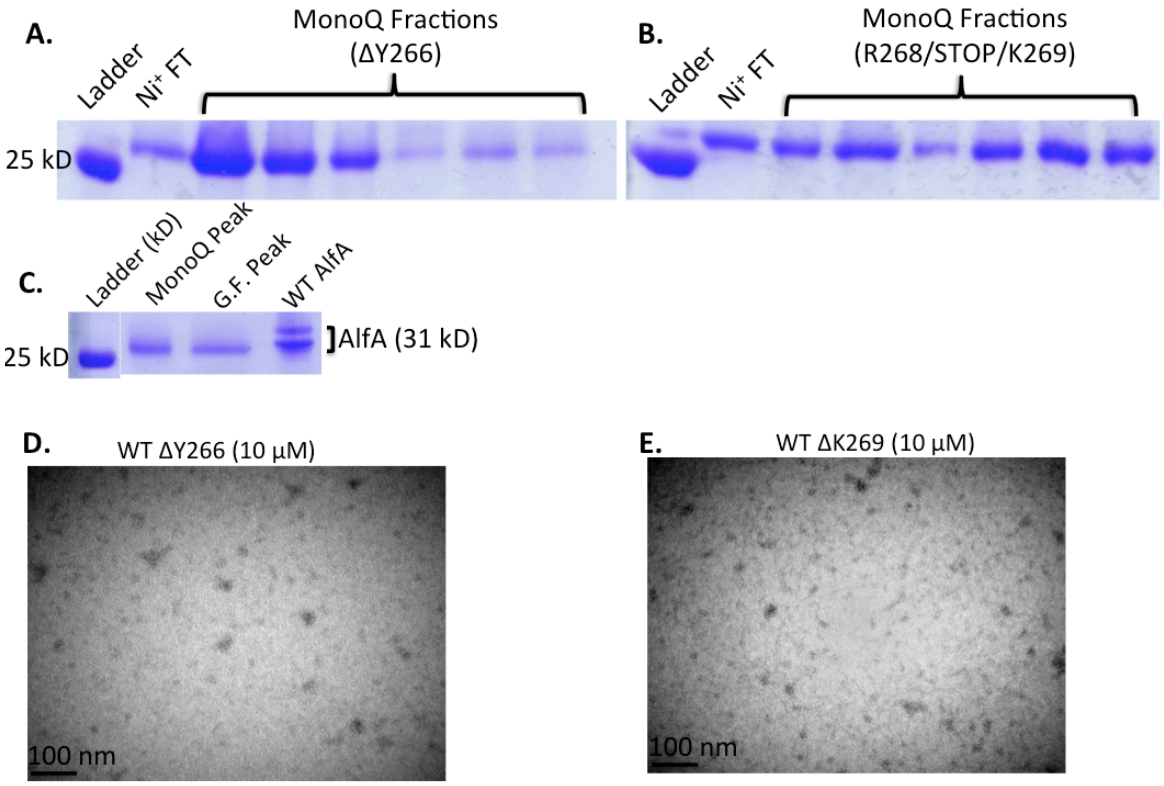

Fig 3.5. A-B: The second NiNTA flow through and the MonoQ fractions of truncation construct ΔY266 (K265/STOP/STOP/Y266) and that of ΔK269 (R268/STOP/K269). C: The purification of ΔY266 using MonoQ and then gel filtration HiLoad 10/300G, running side by side on SDS-PAGE with wild-type AlfA under reducing condition (1 μM BME). D-E: Negative staining TEM micrograph images of the WT ΔY266 and WT ΔK269 with scale bar 100 nm, taken using the T12 microscope.

The polymerization capabilities of the truncation constructs were later examined using negative staining TEM (Figure 3.5D-E). The micrographs show that the wild-type AlfA truncation constructs cannot assemble into filaments.

3.6 Conclusion

Using mass spectrometry, the upper and lower bands of AlfA became less of a mystery. The lower band AlfA was probably the full-length protein. The truncation constructs (ΔY266 and ΔK269) served as additional tools to understand the structure of AlfA. Combined with the optimized FPLC protocol, sufficient quantities of wild-type AlfA and truncation constructs were purified for functional analysis, crystallography and TEM.

Chapter 4: Identifying Polymerization Incompetent Mutants

4.1 Introduction

Now there are tools to purify polymerization incompetent mutants, charge reversal mutations were introduced to certain residues on the barbed end, pointed end, or cross-stranded interface based on the EM reconstruction and homology model (Fig. 1.3B, 1.5). These polymerization incompetent mutants will give insights on how AlfA filaments were assembled, how they were held together, and its functional importance in a biological context.

4.2 Rationales and Design

The polymerization incompetent mutants had two purposes in this study. One of these was to study how AlfA filaments are held together, as discussed in the introduction. Another purpose was to be used in crystallography trials. Dr. Kollman had initially performed a crystal screening using wild-type AlfA, however none of the conditions produced crystals. This was probably because wild-type AlfA tends to form filaments, so the helical contact of filament between subunits might not be compatible with crystal lattice. A protein crystal is an ordered array of repetitive proteins in a 3D structure. Therefore, inhibiting the ability of AlfA to assemble into filaments might promote the crystallization process.

Based on the homology model of AlfA (Fig. 1.3B), charge reversal mutations of amino acids with positively or negative charged R-groups were generated. These charged residues interact with the opposite-charged residues of a nearby subunit. This will hopefully disrupt the interaction of charged residues and prevent polymerization. In

addition, polar uncharged R-group amino acid asparagine side chains can form hydrogen bonds with peptide backbone, and capping hydrogen bond interactions. Therefore, mutation of asparagine would result in the disruption of hydrogen bonds.

At the pointed end (Ib domain) of the AlfA homology model, the designed mutants were (Figure 4.1A): E40K/D41K/E43K, E69K/E70K, and Y42A. At the barbed end (IIa domain), the mutants were: N181D/K186D and D216K/K218D. In addition, there was a mutant R78D/K79D designed at the contact site between Ib domain and Ia domain near the nucleotide-binding site. Most importantly, this mutant is at the cross stranded interface, making contact with a region rich in lysine and alanine on the IIa domain of anti-parallel protofilament strand. In the ParM crystal structure, these two residues are also in contact with the IIb domain.

4.3 Expression and Purifications

Like the wild-type AlfA, the mutants were also expressed in C43 (DE3) cells. It was interesting to note that R78D/K79D and N181D/K186D mutants can also be expressed in BL21 (DE3) cells and have a similar yield to that of expressed in C43 cells. The mutants were then purified with the new protocol with FPLC. One of the mutants, N181D/K186D will not form precipitate during dialysis or concentrating process, thus it was more stable than the wild-type protein. Mutant proteins E69K/E70K and D216K/K218D are less stable than the wild-type protein, since they will form more precipitates during dialysis or concentrating process. The purification of these two mutants could be carried out more easily in buffers containing 0.5 M KCl. The E40K/D41K/E43K mutants are extremely difficult to purify because most of the protein

will turn into precipitates. Attempts were made to optimize the purification of E40K/D41K/E43K mutant by changing the pH, buffer type, glycerol concentrations, salt concentrations, salt type, temperature and combinations of these conditions; but remain to be insoluble in solution.

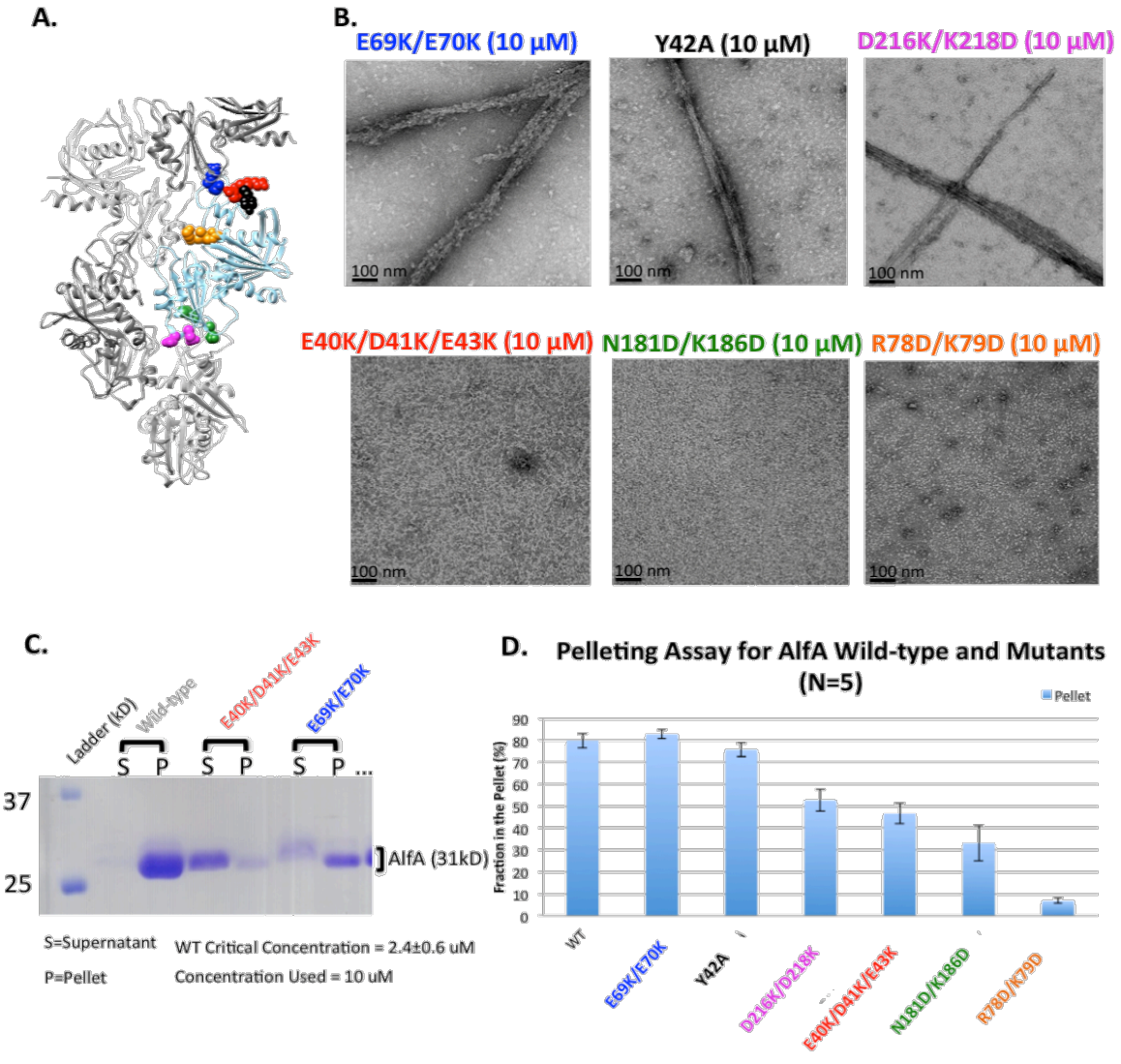

Figure 4.1. A: Homology model of AlfA. B: The negative staining TEM images of polymerization incompetent mutants taken under TF20, scale bar 100 nm. Fig. 4.1 C: Pelleting assay results of polymerization incompetent mutants ran on SDS-PAGE under reducing conditions (1 µM BME), with S being supernatant fraction after centrifugation and P being the pellet fraction after centrifugation. D: Pellet fractions from five different pelleting assay experiments quantified, averaged and illustrated on bar graph with error bars. Control: wild-type AlfA pellet fraction.

4.4 Negative Stain Analysis of Mutants

To test if the mutant proteins were capable of polymerization, assembly reactions were carried out for proteins at concentrations of 10 μM and 100 μM and negative stained. Figure 3.6B shows that at 10 μM some of the mutants were incompetent of polymerization. At 100 μM, the results were same for all the mutants at 10 μM, with the exception of N181D/K186D, which formed filaments.

4.5 Pelleting Assay

To quantify and measure the extent of polymerization for each mutant, pelleting assays were carried out and then ran on SDS-PAGE (Fig. 4.1C). The intensity of the pellet fraction, which was the assembled AlfA, would estimate how much AlfA in the solution were assembled. Using ImageJ, the intensity of the SDS-PAGE bands was collected, averaged, and plotted. Figure 3.6D indicates that the mutant R78D/K79D has the least pellet fraction (at about 5%), while the wild-type AlfA has about 80% pellet fraction.

4.6 Plasmid Loss Assay (PLA)

To further examine the function of AlfA *in vivo*, plasmid loss assays were carried out to assess the stability of the plasmids over a period of long generations, and most importantly, the consequences of plasmid loss. Ideally it would also be necessary to carry out PLA using polymerization incompetent AlfA mutants, but the mutagenesis reactions were not successful.

4.6.1 Determining the Generation Time

Before PLA was carried out, the generation time was determined. Figure 3.7A shows that the average generation times for PY79 cells were 290 minutes at 20°C and 69 minutes at 37°C (Fig. 4.2A-B). The generation time for *Bacillus subtilis* PY79 cells was longer than *E. coli* MG1655 cells, which were 61 minutes on average.

A.

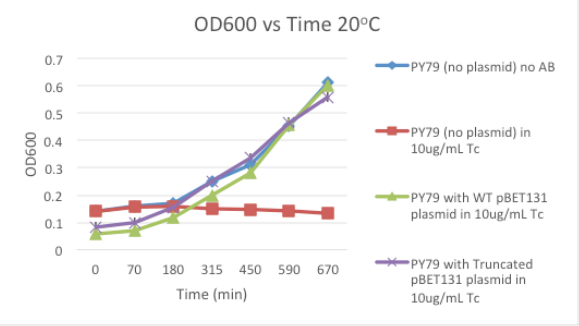

B.

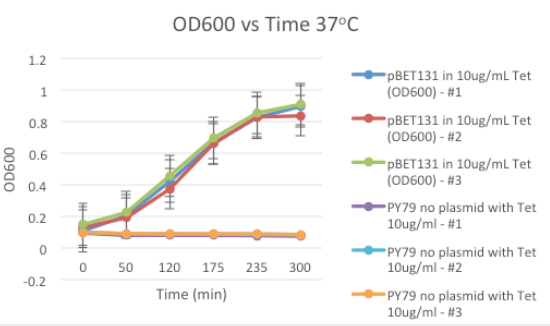

C.

WT AlfA	
Generation #	Loss Rate per Gen (%)
2	0
10	0
20	0
30	0.12

D.

Excised AlfA	
Generation #	Loss Rate per Gen (%)
2	0
10	22.3
20	14.6
30	9.72

Fig 4.2. A: Averaged growth curve of PY79 *Bacillus* cells in 20°C from three experiments. Blue curve indicates PY79 cells without plasmid grown in LB without antibiotics. The red curve indicates PY79 cells with no plasmid gown in antibiotics (10µg/mL tetracycline). The light green curve indicates wild-type pBET131 plasmid in PY79 cells in LB with antibiotics, and purple curve shows the truncated/excised plasmid grown in LB with antibiotics. B: The growth curve of three different PY79 *Bacillus* cells in 37°C, with blue, red, and green curves illustrate the growth of PY79 cells with pBET131. The purple, teal, and orange curves illustrate the growth of PY79 cells without pBET131. C: The loss rate per generation at each generation of PY79 cells transformed with wild-type pBET131 at 37°C. D: The loss rate per generation at each generation of PY79 cells transformed with excised/truncated pBET131 plasmids at 37°C.

4.6.2 Loss Assay Results

The PLA were carried out at 37^{o}C for three times using wild-type pBET131 transformed cells and excised pBET131-transformed cells. In PY79 cells, the loss rate for excised AlfA was significantly higher than wild-type AlfA (Figure 4.2C-D).

4.7 Conclusion

This study now has all the tools for crystallography and hopefully has confirmed how the AlfA filaments are held together, and residues important for polymerization. In addition, the importance of AlfA in a biological context might have been confirmed.

Chapter 5: Crystallization Trials

5.1 Introduction and Background

Protein crystallography is a technique in which proteins are induced to crystalline form by ordered precipitation (Rhodes, 2006). These crystals must be suitable to produce x-ray diffraction patterns, therefore allowing the reconstruction of a protein structure by molecular replacement or anomalous X-ray scattering with selenomethionine. Initially, the purified protein is incubated in screening solutions containing various precipitants that modify the solubility of the protein. These precipitants will hopefully initiate ordered precipitation, crystal nucleation and growth. A lot of variables can affect the outcome of protein crystallization, such as the pH of solutions, different types of buffers, temperatures, solubility, protein entropy, or protein conformations. External chemicals that are not precipitant may also promote crystallography, such as glycerol to modify solubility, reducing agents to prevent oxidation and to mimic *in vivo* environments, nucleotide to induce conformational change, truncation constructs to reduce entropy and disorder within the protein, or co-crystallization with another protein to produce a stable complex (Rhodes, 2006).

5.2 Description of Screens Used

Six screens were used, and each screen contained 96 different conditions. The Classic Suite contained chemicals previously worked for protein crystallization. The Classic II Suite contains the some of the most popular conditions in the Classic Suite plus new reagents such as neutralized organic acids, high concentrations of different salts, and polymers. The Ammonium Sulfate Suite contains solutions of ammonium sulfate with

different salts as co-crystallizers, solutions of ammonium sulfate with different pH conditions and buffer types, and also popular solutions from Biological Macromolecule Crystallization Database (a protein crystallization database) that use ammonium sulfate as the precipitant. The PEGs Suite (polyethylene glycol) contains solutions of PEGS of 200 to 20000, and solutions PEGS3350 with low salts. The JCSG+ Suite contains popular solutions based on the results obtained from the Joint Center for Structural Genomics and European Genomics Consortium, and the conditions usually contain a salt, pH ranging from 4.0-9.0, and also PEGs from 20000 or different MPD concentrations as precipitant. The PACT Suite contains solutions of PEGs 1500 or 6000 in popular biological buffers with different pH, together with or without salts (sodium chloride, ammonium chloride, lithium chloride, magnesium chloride, calcium chloride, and zinc chloride). Preliminary screening is usually done with Classic, Classic II, JCSG, and PACT Suites. If a pattern of crystal hits appears, then additional screens with such as PEGs or $AmSO_4$ Suites are used to narrow down the condition.

5.3 Potential Hits

Despite of the number of trials, there were only a few numbers of potential hits. It was especially difficult to verify if the crystal hits were protein or salt, because AlfA does not have any tryptophan. See Table S1 in the Supplementary for possible hits.

5.4 Optimization Trials

These conditions were optimized using the 24 well plates. Only one of these trials obtained crystal like structures that could be reproduced, this was from Classic II Suite in 0.1 M HEPES pH 7.5, 3.0 M NaCl using wild-type AlfA lower band (Figure 3.3A).

When being reproduced in the 24 well plates (Table S3), the drops appeared to be somewhere in between the state of crystalline and phase separation (Figure 5.1A). So this condition was further optimized using the additive screen, which produced hexagonal crystalline forms (Figure 5.1B-C). Another crystal hit was obtained with WT AlfA purified using the HiTrap column, but this crystal was not reproducible (Fig. 5.1D).

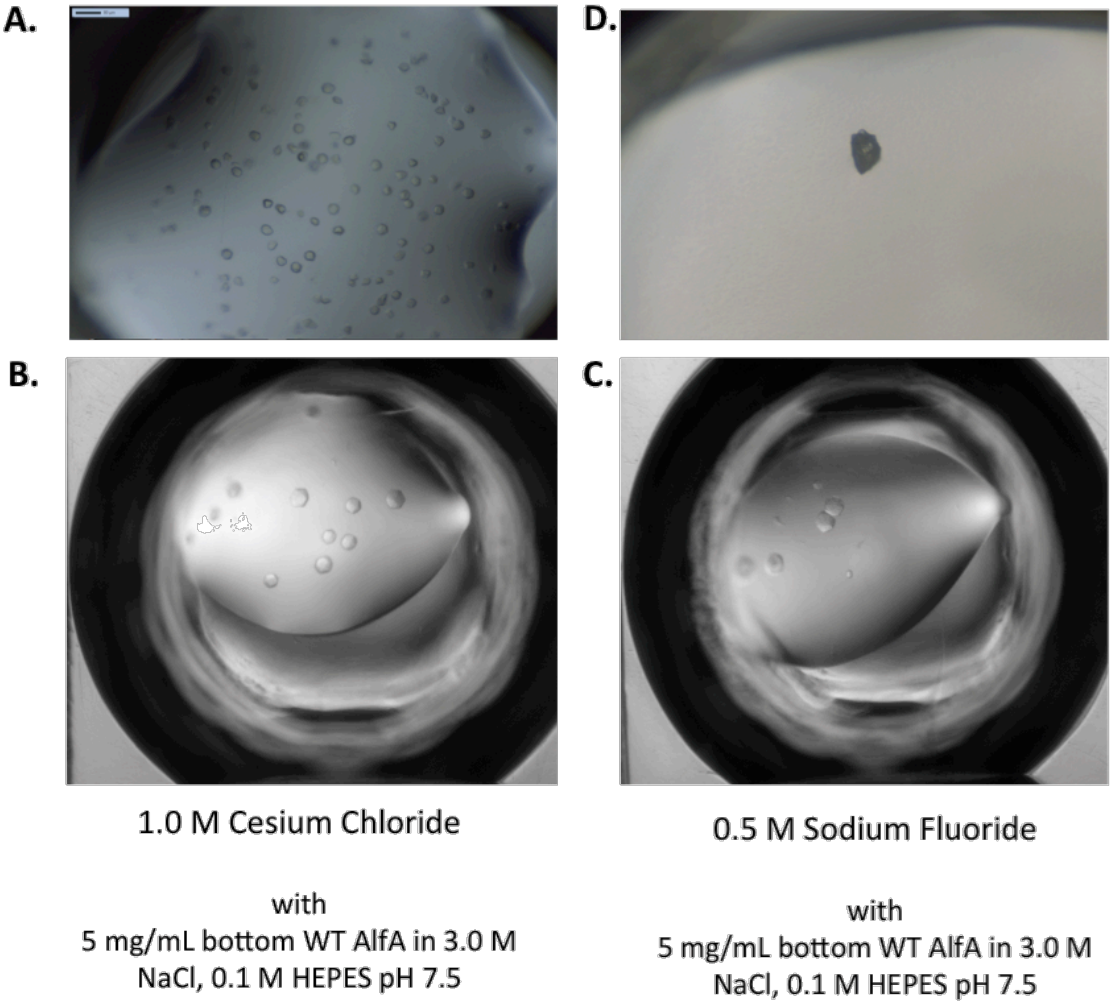

5.1. A: Original crystal hits in 96 well plate with lower band wild-type AlfA 10 mg/mL (1mM DTT) in Classic II screen condition 3.0 M NaCl, 0.1 M HEPES pH 7.5 scale bar 80 µm. B-C: Additive screen optimization of the crystal condition in A using 1.0 M Cesium chloride and 0.5 M Sodium fluoride. Images taken under dissection microscope 10.0X. D: A non-reproducible crystal obtained in 0.1 M Tris-HCL pH 8, 20% MPD with doublet wild-type AlfA 20 mg/mL.

5.5 Diffraction Tests

These crystals from Figure 5.1C-D were shot with 10% glycerol as cryoprotectant (0.1 M HEPES pH 7.5, 3.0 M NaCl, 10% glycerol), but yielded no diffraction. The crystals were also shot at room temperature but yield no diffraction.

5.6 Conclusion

Crystallography trials provided the information that wild-type AlfA (lower band purified by MonoQ) could produce protein crystals, contrary to the previous research. However, the crystals produced by wild-type AlfA needs to be further optimized. The other crystal trials that did not produce crystal will also rule out conditions not capable of producing protein crystals for future research.

Chapter 6 – Discussion

6.1: AlfA Subcloning, Expression, and Purification

6.1.1 Wild-type Purification by FPLC

In Figure 3.1, purified AlfA protein appeared as doublet when ran on SDS-PAGE. This suggests that AlfA were degraded or cleaved during expression or purification. Protocols have been undertaken to inhibit degradation or cleavage, such as the addition of PMSF during purification, or the use of DTT/BME to mimic a reducing environment. However, protein purified with PMSF and/or DTT present still gave a doublet AlfA pattern. It would be helpful if a cocktail of protease inhibitors were used, so it may be possible to conclude that the proteolysis did not take place during purification. Other methods of purification, such as ATP cycling of wild-type AlfA (Figure 4.1C), the doublet pattern also persisted. In another note, C43 (DE3) strains are toxin resistant (Lucigen, 2013), because they might have unknown mechanisms to tolerate foreign proteins. However, when AlfA were expressed in BL21 (DE3) and BL21 (pLYSS) strains the doublet pattern persisted. This suggests that the bacteria strains were probably not responsible for the cleavage. So it remains unclear of how AlfA doublet was formed and additional studies will be required to find out why.

It was strange that singular peaks produced by the HiTrap anion exchange and Superdex200 purifications were doublet AlfA (Figure 3.1BC). Usually, single peak suggests that the protein is monomeric and homogeneous (Abbas, Pichlmair, Gorna, Superti-Furga, & Nagar, 2013). But when the fractions were run on SDS-PAGE, the doublet pattern was seen (Fig. 3.1D). When the same samples were run on a higher percentage SDS-PAGE (15-20%), the doublet bands are still very close together.

It was assumed that the upper band was the full length AlfA, because it ran slower on the SDS-PAGE (larger molecular weight). Likewise, the lower band would assumed to be the degraded product. This hypothesis was rejected by the mass spectrometry results.

6.1.2 Identifying Proteolytic Fragment by Mass Spectrometry

The MonoQ column allows the separation of the lower band from the upper band, and the elution profile evolved into several different peaks. The MonoQ elutions for lower band AlfA were at about the same conductivity to that of HiTrap anion exchange columns. This was probably because MonoQ has higher resolution than the ordinary HiTrap and with a similar anion exchange mechanism (De Cremer K., 2002). When fraction D from Figure 3.2 was ran on a second MonoQ column and then later on gel filtrations, the doublet pattern persisted and it was unclear why (Fig. 3.3CD). Perhaps the upper and lower bands were forming aggregated proteins.

The mass spectrometry results where (R)KFEEmFA and (K)FEEmFA have higher intensity in the lower band than upper band suggested that the upper band might be missing these two peptides. Therefore, the upper band might be the degraded product, and the lower band was actually the full-length product (Fig. 3.4C). This explains why the lower band AlfA can form filament, but upper band cannot (Fig. 3.4AB). A possible explanation where the full-length protein was the lower band on SDS-PAGE was probably because full-length protein has more negative charges so it would run faster (Caprette, 2012).

6.1.3 Designing, Expressing, and Purifying the Truncation Constructs

Neither of the AlfA truncation constructs exhibit doublet pattern before MonoQ purification (Fig. 3.5AB). The EM micrographs (Fig 3.5DE) showed that wild-type AlfA truncation constructs (ΔY266 and ΔK269) cannot assemble into filament, and these results were consistent with the upper AlfA fraction not being able to polymerize (Fig. 3.4A). The result that these two truncation constructs are incompetent to polymerization using negative staining EM suggests that the AlfA doublet might be a result of proteolysis at one of these two disordered C-terminal regions, as suggested by mass spectrometry (Fig. 3.4D). However, Figure 3.5C shows that when the truncation construct was ran side-by-side to doublet AlfA, the migration distance of the truncation construct was equivalent to that of the lower doublet band. This result was contradictory to previous speculations, so more research will be needed to understand this phenomenon. One possibility was that the truncation construct has a different isoelectric point, so it ran differently from the wild-type.

6.1.4 Conclusion

From the introduction, it was unclear if AlfA was degraded or cleaved during purification, and was expected that the upper band was the full-length protein since it ran slower on SDS-PAGE. The truncation construct results supported this initial hypothesis, because the truncation constructs ran at the same position of the lower band.

However, the mass spectrometry results suggested that the upper band was the degradation product. It may be possible that mass spectrometry data from both IRCM and INRS facilities were unreliable, so another mass spectrometry using the truncated construct would help to confirm this speculation.

6.2: Identifying Polymerization Incompetent Mutants

6.2.1 Mutagenesis, Expression, and Purifications

It was interesting how each mutant can behave differently from one another during purification. AlfA was probably toxic to the *E. coli* cells, because of the long protruding bundles formed within the cell. These protruding bundles might disturb normal cell growth and result in more metabolic stress on the cell. The C43 (DE3) cells used to purify wild-type AlfA have tolerance to toxins (Lucigen, 2013). This probably explains why R78D/K79D and N181D/K186D mutants can be expressed in BL21 (DE3), because they have limited capacity to form filaments, so less toxicity and metabolic stress to the cell.

6.2.2 Negative Stain and Pelleting Assay Analysis of Mutants

Figure 4.1D shows that only about 80% of wild-type AlfA assembles, this is normal because the critical concentration of AlfA is 2.4±0.6 μM (Polka et al., 2009). Therefore, only about 24±6% of wild-type AlfA will polymerize, and the pelleting assay results supported this hypothesis.

The negative staining and pelleting assay results indicated that D216K/K218D (pink in Fig. 4.1C), Y42A (black in Fig. 4.1C), and E69K/E70K (blue in Fig. 4.1C) mutants were able to polymerize. Based on the homology model, the D216 site is close together in contact with R68 of another subunit on the same strand, so mutation to lysine should theoretically repel the attraction and prohibit polymerization. However, the K218 was mutated to an alanine, so it probably would not be very effective in prohibiting polymerization. It would be expected that only half (40~50%) of the protein would

assemble. As seen in Figure 4.1D, 50% of the mutant protein assembled, so this result provided some support to the hypothesis. Likewise, for Y42 an aromatic group (tyrosine) was mutated into alanine (nonpolar), and it was initially expected that the mutagenesis could inhibit polymerization. However, because the mutant design were based on a low resolution model, Figure 4.1D shows that almost 80% of the Y42A protein assembled into filaments, a percentage very close to that of the wild-type. In addition, the E69/E70 sites are close together to K186 of another subunits in the same strand, so mutating the glutamate into lysine would theoretically repel the subunit and prevent polymerization. But the results did not support this hypothesis, because Figure 4.1BCD shows that E69K/E70K can form filaments. However, the bundle structures appear to be loosely packed, different from the wild-type AlfA bundles (Fig. 4.1B). This probably suggests that even though the mutation didn't prevent filament assembly; it might have disturbed bundle formation. Changing the pH or salt concentration might restore the wild-type bundle packing.

The N181D/K186D mutant could not form filament at 10 μM, but it was able to form filaments and bundles at 100 μM. Asparagine side chain can form hydrogen bonding with peptide backbones (Yokota et al., 2010), but the mutation was probably not sufficient to inhibit polymerization at higher concentrations. Under negative TEM, these bundles were extremely difficult to find, and about only one bundle structure was present in one grid square. The bundles were also loosely packed as seen previously in E69K/E70K. This probably suggested that the charge attraction between K186 and E69/E70 were important for proper bundle formation. The other mutant site, N181D would theoretically disrupt polymerization somewhere near the assembly contact sites.

This probably explained why this mutant has only limited capacity to form filaments at 10 μM (~30% pellet in Fig. 4.1D), and the difficulty to find bundle structures with 100 μM concentration (~3 mg/mL).

The mutants E40K/D41K/E43K and R78D/K79D were the only two that has not yet observed filament at 10 μM, 100 μM, 5 mg/mL (161 μM) for both mutants, and also 30 mg/mL (968 μM) for R78D/K79D. The maximum concentration that E40K/D41K/E43K could be concentrated to was about 6 mg/mL, so it was not possible to test the polymerization ability at higher than 5 mg/mL. As previously discussed, the residues R78/K79 is near the nucleotide-binding site at the cross-stranded interface to make contact with subunit of the anti-parallel protofilament strand. It could be possible that nucleotide binding will be disrupted when these two residues were mutated, thus becoming incompetent to polymerize (Fig. 4.1). These results supported the hypothesis, because Fig. 4.1D showed that less than 10% of R78D/K79D polymerized. The 10% could be aggregated protein. In ParM, these two residues also make contacts with the IIb domain, and this could suggest that R78D/K79D in AlfA might play a role to compensate for the missing domain during polymerization, but more work would be needed to confirm this speculation.

6.2.4 Plasmid Loss Assay (PLA)

In the introduction, we hypothesized that AlfA polymerization and bundle formation is critical for plasmid segregation. The PLA results of wild-type had a loss rate of 0.12% per generation; this was possible because plasmids are energetically demanding

for the bacteria, so some bacterium might discard their plasmids. A previous study has found that wild-type AlfA in pBET131 has a loss rate of 0.5% after 15 generations (Becker E, 2006). This was a higher loss rate than our results, probably because a different *Bacillus* strain was used, while the PY79 is the strain most resembles wild-type. The results (Fig. 4.2D) for partially truncated AlfA show a significant loss rate of plasmids at 9.72% after 30 generations, which supported the hypothesis that AlfA is critical for plasmid segregation. In conclusion, our results does support the original hypothesis that truncated pBET131 would have a higher loss rate than wild-type plasmids. Unfortunately non-filament forming mutants or non-bundling mutants plasmids could be not generated due to mutagenesis difficulties. These results will allow us to understand whether bundles or filaments are the physiological active polymers, and the effects of losing the ability to form bundles on plasmid inheritance.

6.3: Crystallization Trials

Three of the four crystal hits had monovalent or divalent salts in solution, suggesting a pattern for the crystallization trials using AlfA. This pattern became more apparent when using the salt additive screen, because most of the crystal hits were in wells with soluble fluorides. This pattern could be used for future optimization. The crystallization trials of AlfA using wild-type, polymerization incompetent mutants, and truncation constructs on the C-terminal disorder regions could provide information in future trials, since disordered regions will interfere with crystal lattice formation (Rhodes, 2006). However, the truncation constructs did not produce any hits. Most hits were produced by wild-type AlfA; this could suggest that the helical contact of the filament

was somewhat compatible with crystal lattice geometry, different from initial expectations.

How AlfA compensate for the missing IIb domain remains unclear, because high-resolution crystal structure will be needed to postulate a hypothesis. However, previous research (Polka et al., 2009) suggested that AlfA filaments are highly twisted (40^{o}) with left-handedness, so it might be possible that the higher angle twist might stabilized the filament and serve as a mechanism to compensate for the missing domain. Our higher resolution cryo-EM model also confirmed this high twist in the AlfA structure. The twist angle has significance because eukaryotic actin had a right-handed twist of 27^{o} (Fujii et al., 2010), while the ParM from R1 plasmids in *E. coli* had a 30^{o} left-handed twist (Galkin, Orlova, Schroder, & Egelman, 2010), and therefore making the highly twisted model of AlfA unique. Despite of these speculations, more research will be required to confirm this hypothesis.

6.4: Future Directions

6.4.1 Purification Strategy

It could be possible to purify the ULP1 by FPLC, so the AlfA would have fewer impurities during crystallization trials. Additionally, it could be possible to subclone additional histidine tags onto ULP1, so that the AlfA would be of a higher purity. This will allow using less Ni+NTA resin during purification to save time and funding.

Most importantly, it would be a priority to find out why truncated AlfA run in the same position as lower band wild-type AlfA on SDS-PAGE

(Fig. 3.5C). It would also be interesting to find out how and why was wild-type AlfA split into the doublet, possibly by using cocktails of protease inhibitors.

6.4.2 Mutants and Truncation Constructs

The E69K/E70K mutants can form filaments but the bundles were loosely packed (Fig. 4.1B) than the wild-type. If changing the pH or salt concentration does not restore the wild-type packing, it might be interesting to use techniques such as ITC to study the effects on bundle formation due to these mutated residues. Using ITC, if the E69K/E70K mutant could have lower activation energy than wild-type AlfA, this could potentially suggest that E69K/E70K are indeed loosely packed (or in a different conformation) as the wild-type.

Additional mutants can be generated for crystallography trials. New truncation constructs at the C-terminus could be used for crystallography trials. It might not be necessary to generate truncation constructs at the N-terminus, but it could remain as a possibility for more crystallography trials.

6.4.3 Pelleting Assay

Additional pelleting assays could be performed using AlfA wild-type, mutants and truncation constructs at different pH, salt concentration, or in a different salt (e.g. NaCl) to study their effects on polymerization. *Bacillus* will undergoes starvation to produce spores when the growth condition becomes unfavorable, and this could be due to extreme pH, high salt or low nutrients. Conducting pelleting assays at these conditions will better our understanding of AlfA's assembly dynamic in different unfavorable growth environments.

6.4.4 Plasmid Loss Assay

Plasmid loss assay using the polymerization incompetent mutants, non-bundle forming mutants, or truncation constructs can be performed to understand the role of AlfA filaments and bundles during plasmid segregation. PLA at unfavorable growth condition using wild-type AlfA or mutants could also be done to study the role of AlfA under cellular stress, or the role of AlfA during sporulation. Due to previous failed attempts of mutagenesis PCR using different protocols and polymerases, it might just be easier and cost-efficient to synthesize the mutated plasmids in the future. Alternatively, it could be possible to conduct PLA using a smaller plasmid pEB255, which contain the AlfA and its surrounding regions and have a similar wild-type loss rate to pBET131 (Becker E, 2006). Mutagenesis PCR might be easier in a smaller plasmid.

It was interesting to observe that the loss rate per generation was higher at 10^{th} generation (22.3%) and lower at 30^{th} generation (9.72%). All three trials of this experiment showed consistent results. It was unclear how this might have happened, but it could be possible the bacteria can detect the loss of plasmid so they developed mechanisms to help segregate pBET131. It might also be possible that AlfA-like mechanisms are already present in the bacteria, which can ensure plasmid inheritance. However these speculations will definitely need to be tested in future experiments.

6.4.5 Crystal Optimization and Diffraction Tests

Crystal optimization could be done using the soluble fluorides in the additive screen. It may also be possible to use additional NeXtal screens or to make personalized 96-well screens for encouraging better crystallization conditions. A personalized 96-well

screen containing low molecular weight PEGs, 30% MPD, salts in HEPEs, soluble fluorides or a combination of these could be useful to screen for more crystallization conditions. Diffractions tests of these crystal conditions could be carried out at room temperature, or without cryo-protectant. It could also be possible to expose the crystal with different exposure times. Additionally, seeding techniques could be used to encourage growth of crystals (Rhodes, 2006).

6.4.6 Quad Mutants and Cryo-ET of Bundles

Dr. Kollman is currently working on improving the resolution obtained using the cryo-EM data of non-bundle forming (Quad) mutants using different reconstruction algorithms. These purified quad mutants could also be used in crystallography trials. The cryo-ET of AlfA bundles and E69K/E70K mutant could help our understanding of the AlfA during plasmid segregation, and how the filaments came together to form the bundles. An approach using correlative cryo-ET with fluorescence microscopy would be very interesting to see the role of AlfA plasmid segregation *in vivo*.

6.5 Conclusion

Most research goals have been met and we are now able to understand the role of AlfA better than before. We have made progress in understanding plasmid segregation, but the limitation of EM and the inability to perform X-ray crystallography on filamentous proteins significantly reduces the resolution of our actin models. However, with improvements in EM reconstruction algorithms and the innovation of direct detection camera, more can be understood about the structural contact of AlfA polymers

on its propensity to form bundled structures. Future research will take advantage of this progress to determine the molecular mechanism of plasmid segregation.

References

Abbas, Y. M., Pichlmair, A., Gorna, M. W., Superti-Furga, G., & Nagar, B. (2013). Structural basis for viral 5'-PPP-RNA recognition by human IFIT proteins. *Nature, 494*(7435), 60-64. doi: 10.1038/nature11783

Agilent. (2013, Oct 5). QuikChange XL Site-Directed Mutagenesis Kit. Retrieved Jan 1, 2015, from https://www.genomics.agilent.com/literature.jsp?crumbAction=push&tabId=AG-PR-1160&contentType=User+Manual

Aylett, C. H., Wang, Q., Michie, K. A., Amos, L. A., & Lowe, J. (2010). Filament structure of bacterial tubulin homologue TubZ. *Proc Natl Acad Sci U S A, 107*(46), 19766-19771. doi: 10.1073/pnas.1010176107

Becker E, H. N., Gunderson FQ, Derman AI, Dance AL, Sims J, Larsen RA, Pogliano J. (2006). DNA segregation by the bacterial actin AlfA during Bacillus subtilis growth and development. *EMBO, 25*(24), 5919-5931. doi: 10.1038/sj.emboj.7601443

Becker, W. M., Kleinsmith, L.J., Hardin, J., and Bertoni, G.P. . (2009). *The World of the Cell 7th Edition*. San Francisco: Pearson Benjamin Cummings.

Bennett, P. M. (2008). Plasmid encoded antibiotic resistance: acquisition and transfer of antibiotic resistance genes in bacteria. *Br J Pharmacol, 153 Suppl 1*, S347-357. doi: 10.1038/sj.bjp.0707607

Bertram Katzung, S. M., Anthony Trevor. (2012). *Basic and Clinical Pharmacology* (12 ed.): McGraw-Hill Medical.

Bharat, T. A., Murshudov, G. N., Sachse, C., & Lowe, J. (2015). Structures of actin-like ParM filaments show architecture of plasmid-segregating spindles. *Nature*, 1-5. doi: 10.1038/nature14356

Cambridge. (2008). Bacillus subtilis Transformation. Retrieved May, 2014, from http://2008.igem.org/Team:Cambridge/Bacillus_subtilis_transformation

Campbell, C. S., & Mullins, R. D. (2007). In vivo visualization of type II plasmid segregation: bacterial actin filaments pushing plasmids. *J Cell Biol, 179*(5), 1059-1066. doi: 10.1083/jcb.200708206

Campbell, N. A. (1996). *Biology* (J. Schmid Ed. 4th ed.). USA: The Benjamin/Cummings.

Caprette, D. (2012). Introduction to SDS-PAGE. Retrieved September, 2013, from http://www.ruf.rice.edu/~bioslabs/studies/sds-page/gellab2.html

Carballido-Lopez, R. (2006). The bacterial actin-like cytoskeleton. *Microbiol Mol Biol Rev, 70*(4), 888-909. doi: 10.1128/MMBR.00014-06

De Cremer K., C. R., Strijckmans K., Dams R., Lameire N., and Vanholder R. (2002). Behaviour of vanadate and vanadium–transferrin complex on different anion-exchange columns. Application to in vivo 48V-labelled rat serum. *Journal of Chromatography B, 775*, 143-152.

del Solar, G., Giraldo, R., Ruiz-Echevarría, M., Espinosa, M., & Díaz-Orejas, R. (1998). Replication and Control of Circular Bacterial Plasmids. *Microbiol Mol Biol Rev, 62*(2), 434-464.

Dominguez, R., & Holmes, K. C. (2011). Actin structure and function. *Annu Rev Biophys, 40*, 169-186. doi: 10.1146/annurev-biophys-042910-155359

Dos Remedios, C. G., Chhabra, D., Kekic, M., Dedova, I.V., Tsubakihara, M., Berry, D.A., and Nosworthy, N.J. . (2002). Actin Binding Proteins- Regulation of Cytoskeletal Microfilaments. *Physiol Rev, 83*, 433-473.

Egelman, E. (2003). Actin's prokaryotic homologs. *Current Opinion in Structural Biology, 13*(2), 244-248. doi: 10.1016/s0959-440x(03)00027-7

Egelman, E. H. (2003). A tale of two polymers: new insights into helical filaments. *Nat Rev Mol Cell Biol, 4*(8), 621-630. doi: 10.1038/nrm1176

Fujii, T., Iwane, A. H., Yanagida, T., & Namba, K. (2010). Direct visualization of secondary structures of F-actin by electron cryomicroscopy. *Nature, 467*(7316), 724-728. doi: 10.1038/nature09372

Funnell, J. A. S. a. B. E. (2003). Plasmid and Chromosome Traffic Control: How ParA and ParB Drive Partition. *Current Topics in Developmental Biology, 56*, 145-180.

Galkin, V. E., Orlova, A., Rivera, C., Mullins, R. D., & Egelman, E. H. (2009). Structural polymorphism of the ParM filament and dynamic instability. *Structure, 17*(9), 1253-1264. doi: 10.1016/j.str.2009.07.008

Galkin, V. E., Orlova, A., Schroder, G. F., & Egelman, E. H. (2010). Structural polymorphism in F-actin. *Nat Struct Mol Biol, 17*(11), 1318-1323. doi: 10.1038/nsmb.1930

Galkin, V. E., Orlova, A., Vos, M. R., Schroder, G. F., & Egelman, E. H. (2015). Near-atomic resolution for one state of f-actin. *Structure, 23*(1), 173-182. doi: 10.1016/j.str.2014.11.006

Garner, E. C., Campbell, C.S., and Mullins, R.D. . (2004). Dynamic Instability in a DNA-Segregating Prokaryotic Actin Homolog. *Science, 306*, 109-114.

Garner, E. C., Campbell, C.S., Weibel, D.B., and Mullins, R.D. (2007). Reconstitution of DNA Segregation Driven by Assembly of a Prokaryotic Actin Homolog. *Science, 315*, 1270-1274.

Garner EC, C. C., Mullins RD. (2004). Dynamic instability in a DNA-segregating prokaryotic actin homolog. *Science, 306*. doi: 10.1126/science.1101313

Goode, B. L., Rodal, A.A., Barnes, G., and Drubin, D.G. . (2001). Activation of the Arp2:3 Complex by the Actin Filament Binding Protein Abp1p. *The Journal of Cell Biology, 153*(3), 627-634.

Heidelberg, J. F., Paulsen, I. T., Nelson, K. E., Gaidos, E. J., Nelson, W. C., Read, T. D., . . . Fraser, C. M. (2002). Genome sequence of the dissimilatory metal ion-reducing bacterium Shewanella oneidensis. *Nat Biotechnol, 20*(11), 1118-1123. doi: 10.1038/nbt749

Jensen, R. B., and Gerdes, K. . (1997). Partitioning of plasmid R1. The ParM protein exhibits ATPase activity and interacts with the centromere-like ParR-parC complex. *Journal of Molecular Biology*(269), 505-513.

Jones, K. L., Kim, S. W., & Keasling, J. D. (2000). Low-copy plasmids can perform as well as or better than high-copy plasmids for metabolic engineering of bacteria. *Metab Eng, 2*(4), 328-338. doi: 10.1006/mben.2000.0161

Kenn Gerdes, J. M. l.-J. a. R. B. J. (2000). Plasmid and chromosome partitioning: surprises from phylogeny. *Molecular Microbiology, 37*(3), 455-466.

Lewis, A. K., and Bridgman, P.C. . (1992). Nerve Growth Cone LameUipodia Contain Two Populations of Actin Filaments That Differ in Organization and Polarity *The Journal of Cell Biology, 119*(5), 1219-1243.

Lima, C. D. (2009). United States of America Patent No. 6,872,551. Memorial Sloan-Kettering Cancer Center.

Lucigen. (2013). C41(DE3) and C43(DE3) Competent Cells. Retrieved September, 2013, from http://lucigen.com/OverExpress-C41-DE3-and-C43-DE3-Competent-Cells/

Makarova, K. S., Wolf, Y. I., & Koonin, E. V. (2009). Comprehensive comparative-genomic analysis of type 2 toxin-antitoxin systems and related mobile stress response systems in prokaryotes. *Biol Direct, 4*, 19. doi: 10.1186/1745-6150-4-19

Marshall, K. M., Bradshaw, M., Pellett, S., and Johnson, E.A. . (2007). Plasmid Encoded Neurotoxin Genes in Clostridium botulinum Serotype A Subtypes. *Biochem Biophysics Res Commun., 361*(1), 49-54.

McGough, A., Pope, B., Chiu, W., & Weeds, A. (1997). Cofilin changes the twist of F-actin: implications for actin filament dynamics and cellular function. *J Cell Biol, 138*(4), 771-781.

McManus, M. (2013). Rubidium Chloride Competent Cell Protocol. Retrieved Sept., 2013, from http://mcmanuslab.ucsf.edu/protocol/rubidium-chloride-competent-cell-protocol

Møller-Jensen, J., Borch, J., Dam, M., Jensen, R.B., Roepstorff, P., and Gerdes, K. . (2003). Bacterial Mitosis- ParM of Plasmid R1 Moves Plasmid DNA by an Actin-like Insertional Polymerization Mechanism. *Molecular Cell, 12*, 1477-1487.

Møller-Jensen, J., Ringgaard, S., Mercogliano, C.P., Gerdes, K., and Löwe, J. (2007). Structural analysis of the ParR:parC plasmid partition complex. *EMBO, 26*, 4413-4422. doi: 10.1038/

Møller‐Jensen, J., Jensen, R. B., Löwe, J., & Gerdes, K. (2002). *Prokaryotic DNA segregation by an actin‐like filament* (Vol. 21).

Nakabachi A, Y. A., Toh H, Ishikawa H, Dunbar HE, Moran NA, Hattori M. (2007). The 160-Kilobase Genome of the Bacterial Endosymbiont Carsonella. *Science, 314*(5797).

Nanuq. (2013). How to Submit Samples. Retrieved October, 2013, from http://gqinnovationcenter.com/documents/sequencing/howToSubmitSamplesTutorial_en.pdf

NEB. (2015). Site Directed Mutagenesis. Retrieved March, 2015, from https://www.neb.com/applications/cloning-and-synthetic-biology/site-directed-mutagenesis

Otterbein, L. R., Graceffa, P., and Dominguez, R. . (2001). The crystal structure of uncomplexed actin in the ADP state. *Science, 293*, 708-711.

Ozyamak, E., Kollman, J., Agard, D. A., & Komeili, A. (2013). The bacterial actin MamK: in vitro assembly behavior and filament architecture. *J Biol Chem, 288*(6), 4265-4277. doi: 10.1074/jbc.M112.417030

Ozyamak, E., Kollman, J. M., & Komeili, A. (2013). Bacterial actins and their diversity. *Biochemistry, 52*(40), 6928-6939. doi: 10.1021/bi4010792

Pettersen, E. F., Goddard, T. D., Huang, C. C., Couch, G. S., Greenblatt, D. M., Meng, E. C., & Ferrin, T. E. (2004). UCSF Chimera--a visualization system for exploratory research and analysis. *J Comput Chem, 25*(13), 1605-1612. doi: 10.1002/jcc.20084

Polka, J. K., Kollman, J. M., Agard, D. A., & Mullins, R. D. (2009). The structure and assembly dynamics of plasmid actin AlfA imply a novel mechanism of DNA segregation. *J Bacteriol, 191*(20), 6219-6230. doi: 10.1128/JB.00676-09

Polka, J. K., Kollman, J. M., & Mullins, R. D. (2014). Accessory factors promote AlfA-dependent plasmid segregation by regulating filament nucleation, disassembly, and bundling. *Proc Natl Acad Sci U S A, 111*(6), 2176-2181. doi: 10.1073/pnas.1304127111

Popp, D., Narita, A., Lee, L. J., Ghoshdastider, U., Xue, B., Srinivasan, R., . . . Robinson, R. C. (2012). Novel actin-like filament structure from Clostridium tetani. *J Biol Chem, 287*(25), 21121-21129. doi: 10.1074/jbc.M112.341016

Pradella, S., Hans, A., Sproer, C., Reichenbach, H., Gerth, K., & Beyer, S. (2002). Characterisation, genome size and genetic manipulation of the myxobacterium Sorangium cellulosum So ce56. *Arch Microbiol, 178*(6), 484-492. doi: 10.1007/s00203-002-0479-2

Rhodes, G. (2006). *Crystallography Made Crystal Clear* (3rd ed.). Canada: Elsevier.

Salje, J., Gayathri, P., & Lowe, J. (2010). The ParMRC system: molecular mechanisms of plasmid segregation by actin-like filaments. *Nat Rev Microbiol, 8*(10), 683-692. doi: 10.1038/nrmicro2425

Salje, J., Zuber, B., and Löwe, J. (2009). Electron Cryomicroscopy of E. coli Reveals Filament Bundles Involved in Plasmid DNA Segregation. *2009, 179*, 509-512.

Sengupta, M., & Austin, S. (2011). Prevalence and significance of plasmid maintenance functions in the virulence plasmids of pathogenic bacteria. *Infect Immun, 79*(7), 2502-2509. doi: 10.1128/IAI.00127-11

Shaevitz, J. W., & Gitai, Z. (2010). The structure and function of bacterial actin homologs. *Cold Spring Harb Perspect Biol, 2*(9), a000364. doi: 10.1101/cshperspect.a000364

Shearer, J. E., Wireman, J., Hostetler, J., Forberger, H., Borman, J., Gill, J., . . . Summers, A. O. (2011). Major families of multiresistant plasmids from geographically and epidemiologically diverse staphylococci. *G3 (Bethesda), 1*(7), 581-591. doi: 10.1534/g3.111.000760

Shukla, H. D., & Sharma, S. K. (2005). Clostridium botulinum: a bug with beauty and weapon. *Crit Rev Microbiol, 31*(1), 11-18. doi: 10.1080/10408410590912952

Stephens, C. (1998). Bacterial sporulation: A question of commitment? *Current Biology, 8*(2). doi: 10.1016/S0960-9822(98)70031-4

Tanaka, T. (2010). Functional analysis of the stability determinant AlfB of pBET131, a miniplasmid derivative of bacillus subtilis (natto) plasmid pLS32. *J Bacteriol, 192*(5), 1221-1230. doi: 10.1128/JB.01312-09

Teruo Tanaka, M. O. (1998). A novel Bacillus natto plasmid pLS32 capable of replication in Bacillus subtilis. *FEBS, 422*(2), 243-246. doi: doi:10.1016/S0014-5793(98)00015-5

van den Ent F, A. L., Löwe J. (2001). Prokaryotic origin of the actin cytoskeleton. *Nature, 413*, 39-44.

van den Ent, F., Izore, T., Bharat, T. A., Johnson, C. M., & Lowe, J. (2014). Bacterial actin MreB forms antiparallel double filaments. *Elife, 3*, e02634. doi: 10.7554/eLife.02634

van den Ent, F., & Löwe, J. (2000). *Crystal structure of the cell division protein FtsA from Thermotoga maritima* (Vol. 19).

van den Ent, F., Møller‐Jensen, J., Amos, L. A., Gerdes, K., & Löwe, J. (2002). *F‐actin‐like filaments formed by plasmid segregation protein ParM* (Vol. 21).

Winder, S. J., & Ayscough, K. R. (2005). Actin-binding proteins. *J Cell Sci, 118*(Pt 4), 651-654. doi: 10.1242/jcs.01670

Yokota, A., Tsumoto, K., Shiroishi, M., Nakanishi, T., Kondo, H., & Kumagai, I. (2010). Contribution of asparagine residues to the stabilization of a proteinaceous antigen-antibody complex, HyHEL-10-hen egg white lysozyme. *J Biol Chem, 285*(10), 7686-7696. doi: 10.1074/jbc.M109.089623

Zheng, L., Baumann, U., & Reymond, J. L. (2004). An efficient one-step site-directed and site-saturation mutagenesis protocol. *Nucleic Acids Res, 32*(14), e115. doi: 10.1093/nar/gnh110

Supplementary Material

Table S1: All crystals obtained from screening.

Screen	Well	Protein	WT/Mut	Concentration(s) (mg/mL)	Substrate (s)	Temperature (°C)	Apparence	X-ray Diffraction
JCSG+	F1	Doublet	R78D/K79D	10	None	22	Solid Chunk	Salt Crystal Diffraction
Classic	A10	Doublet	R78D/K79D	5, 10	None	4	Solid Chunk	
Classic II	E6	Doublet	Wildtype	10, 20	None	22	Needles	
Classic II	E6	Doublet	R78D/K79D	10	None	22	Needles	
Classic II	E6	Doublet	R78D/K79D	10	1mM ADP	4	Needles	
Classic II	D12	Doublet	R78D/K79D	5	None	4	Needles	
Classic II	D12	Doublet	R78D/K79D	5	1mM ADP	4	Needles	
Classic II	A11	Lower Band	Wildtype	5, 10	None	22	Circular Crystals	No Diffraction
JCSG+	D8	ΔY266	R78D/K79D	7.5	1mM ADP	4	Needles	
Hampton Additive	B7	Lower Band	Wildtype	5, 7.5, 10	None	22	Hexagonal Crystals	No Diffraction
	B12	Lower Band	Wildtype	5, 7.5, 10	None	22	Hexagonal Crystals	No Diffraction

Table S2: All crystallizaion conditions performed.

Protein	WT/Mut	Screen	Additive(s)	Concentration(s) (mg/mL)	Temperature (°C)	Substrate(s)	General Observation
Buffer	N/A	Classic	None	N/A	22	None	Clear
Buffer	N/A	Classic II	None	N/A	22	None	Clear
Buffer	N/A	JCSG+	None	N/A	22	None	Clear
Buffer	N/A	PEGs	None	N/A	22	None	Clear
Buffer	N/A	AmSO4	None	N/A	22	None	Clear
Buffer	N/A	PACT	None	N/A	22	None	Clear
Doublet	Wildtype	Classic	None	5 | 10 | 20	4 | 22	None | ATP | ADP | AMP-PNP	The wells contained 90% precipitates, 5% phase separation, and 5% clear without substrate. With ATP and AMP-PNP, 80% of wells contained precipitates, 5% phase separation and 15% clear. The addition of ADP solublized proteins, such that 70% are precipitates, 5% phase separation and 25% clear. WT with nucleotide assembled into filament in protein buffer.
Doublet	Wildtype	Classic II	None	5 | 10 | 20	4 | 22	None | ATP | ADP | AMP-PNP	
Doublet	Wildtype	JCSG+	None	5 | 10 | 20	4 | 22	None | ATP | ADP | AMP-PNP	
Doublet	Wildtype	PEGs	None	5 | 10 | 20	4 | 22	None | ATP | ADP | AMP-PNP	
Doublet	Wildtype	AmSO4	None	5 | 10 | 20	4 | 22	None | ATP | ADP | AMP-PNP	
Doublet	R78D/K79D	Classic	None	5 | 10 | 20	4 | 22	None | ATP | ADP | AMP-PNP	
Doublet	R78D/K79D	Classic II	None	5 | 10 | 20	4 | 22	None | ATP | ADP | AMP-PNP	
Doublet	R78D/K79D	JCSG+	None	5 | 10 | 20	4 | 22	None | ATP | ADP | AMP-PNP	
Doublet	R78D/K79D	PEGs	None	5 | 10 | 20	4 | 22	None | ATP | ADP | AMP-PNP	
Doublet	R78D/K79D	AmSO4	None	5 | 10 | 20	4 | 22	None | ATP | ADP | AMP-PNP	
Doublet	Wildtype	Classic	None	5 | 10 | 20	4 | 22	None | 5% Glycerol	Glycerol reduced solubility of the protein, with 95% of wells with precipitates and 5% phase separation. None of the wells were clear.
Doublet	Wildtype	Classic II	None	5 | 10 | 20	4 | 22	None | 5% Glycerol	
Doublet	Wildtype	JCSG+	None	5 | 10 | 20	4 | 22	None | 5% Glycerol	
Doublet	Wildtype	PEGs	None	5 | 10 | 20	4 | 22	None | 5% Glycerol	
Doublet	Wildtype	AmSO4	None	5 | 10 | 20	4 | 22	None | 5% Glycerol	
Doublet	R78D/K79D	Classic	None	5 | 10 | 20	4 | 22	None | 5% Glycerol	

Protein	WT/Mut	Screen	Additive(s)	Concentration(s) (mg/mL)	Temperature (°C)	Substrate(s)	General Observation
Doublet	R78D/K79D	Classic II	None	5 | 10 | 20	4 | 22	None | 5% Glycerol	Glycerol reduced solubility of the protein, with 95% of wells with precipitates and 5% phase separation. None of the wells were clear.
Doublet	R78D/K79D	JCSG+	None	5 | 10 | 20	4 | 22	None | 5% Glycerol	
Doublet	R78D/K79D	PEGs	None	5 | 10 | 20	4 | 22	None | 5% Glycerol	
Doublet	R78D/K79D	AmSO4	None	5 | 10 | 20	4 | 22	None | 5% Glycerol	
Doublet	Wildtype	Classic	None	5 | 10 | 20	4 | 22	ADP | ADP+5% Glycerol	90% precipitates, 5% phase separation and 5% clear.
Doublet	Wildtype	Classic II	None	5 | 10 | 20	4 | 22	ADP | ADP+5% Glycerol	
Doublet	Wildtype	JCSG+	None	5 | 10 | 20	4 | 22	ADP | ADP+5% Glycerol	
Doublet	Wildtype	PEGs	None	5 | 10 | 20	4 | 22	ADP | ADP+5% Glycerol	
Doublet	Wildtype	AmSO4	None	5 | 10 | 20	4 | 22	ADP | ADP+5% Glycerol	
Doublet	R78D/K79D	Classic	None	5 | 10 | 20	4 | 22	ADP | ADP+5% Glycerol	
Doublet	R78D/K79D	Classic II	None	5 | 10 | 20	4 | 22	ADP | ADP+5% Glycerol	
Doublet	R78D/K79D	JCSG+	None	5 | 10 | 20	4 | 22	ADP | ADP+5% Glycerol	
Doublet	R78D/K79D	PEGs	None	5 | 10 | 20	4 | 22	ADP | ADP+5% Glycerol	
Doublet	R78D/K79D	AmSO4	None	5 | 10 | 20	4 | 22	ADP | ADP+5% Glycerol	
Doublet	E40K/D41K/E43K	Classic	None	2.5 | 5 | 7	4 | 22	None | ADP	Most wells are cloudy or precipitated (95%). Other 5% wells were clear, and wells with ADP did not have better solubility. Given that Mut E40K/D41K/E43K is not stable in protein buffer, the highest concentration used in crystallization trial was 7.0 mg/mL.
Doublet	E40K/D41K/E43K	Classic II	None	2.5 | 5 | 7	4 | 22	None | ADP	
Doublet	E40K/D41K/E43K	JCSG+	None	2.5 | 5 | 7	4 | 22	None | ADP	
Doublet	E40K/D41K/E43K	PEGs	None	2.5 | 5 | 7	4 | 22	None | ADP	
Doublet	E40K/D41K/E43K	AmSO4	None	2.5 | 5 | 7	4 | 22	None | ADP	
Doublet	E40K/D41K/E43K	PACT	None	2.5 | 5 | 7	4 | 22	None | ADP	

Protein	WT/Mut	Screen	Additive(s)	Concentration(s) (mg/mL)	Temperature (°C)	Substrate(s)	General Observation
Doublet	N181D/K186D	Classic	None	5 | 7.5 | 10	4 | 22	None | ADP	Without ADP, 80% of wells contained precipitates, and 20% were clear. There was no phase separation. Wells with ADP have better solubility, with 70% of wells containing precipitates and 30% clear.
Doublet	N181D/K186D	Classic II	None	5 | 7.5 | 10	4 | 22	None | ADP	
Doublet	N181D/K186D	JCSG+	None	5 | 7.5 | 10	4 | 22	None | ADP	
Doublet	N181D/K186D	PEGs	None	5 | 7.5 | 10	4 | 22	None | ADP	
Doublet	N181D/K186D	AmSO4	None	5 | 7.5 | 10	4 | 22	None | ADP	
Doublet	N181D/K186D	PACT	None	5 | 7.5 | 10	4 | 22	None | ADP	
Upper Band	Wildtype	Classic	None	5 | 7.5 | 10	4 | 22	None | ATP | ADP | AMP-PNP	80% precipitates, 20% clear without substrate. With ADP, 60% of wells had precipitates and 40% of wells were clear.
Upper Band	Wildtype	Classic II	None	5 | 7.5 | 10	4 | 22	None | ATP | ADP | AMP-PNP	
Upper Band	Wildtype	JCSG+	None	5 | 7.5 | 10	4 | 22	None | ATP | ADP | AMP-PNP	
Upper Band	Wildtype	PEGs	None	5 | 7.5 | 10	4 | 22	None | ATP | ADP | AMP-PNP	
Upper Band	Wildtype	AmSO4	None	5 | 7.5 | 10	4 | 22	None | ATP | ADP | AMP-PNP	
Upper Band	Wildtype	PACT	None	5 | 7.5 | 10	4 | 22	None | ATP | ADP | AMP-PNP	
Lower Band	Wildtype	Classic	None	5 | 7.5 | 10	4 | 22	None | ATP | ADP | AMP-PNP | GTP	
Lower Band	Wildtype	Classic II	None	5 | 7.5 | 10	4 | 22	None | ATP | ADP | AMP-PNP | GTP	
Lower Band	Wildtype	JCSG+	None	5 | 7.5 | 10	4 | 22	None | ATP | ADP | AMP-PNP | GTP	
Lower Band	Wildtype	PEGs	None	5 | 7.5 | 10	4 | 22	None | ATP | ADP | AMP-PNP | GTP	
Lower Band	Wildtype	AmSO4	None	5 | 7.5 | 10	4 | 22	None | ATP | ADP | AMP-PNP | GTP	

Protein	WT/Mut	Screen	Additive(s)	Concentration(s) (mg/mL)	Temperature (°C)	Substrate(s)	General Observation
Lower Band	Wildtype	PACT	None	5 | 7.5 | 10	4 | 22	None | ATP | ADP | AMP-PNP | GTP	80% precipitates, 20% clear without substrate.
Lower Band	Wildtype	Classic	CaCl2	5 | 7.5 | 10	4 | 22	None	Added CaCl2 as an additive out of curiosity, and all of the wells were cloudy or with precipitates.
Lower Band	Wildtype	Classic II	CaCl2	5 | 7.5 | 10	4 | 22	None	
Lower Band	Wildtype	JCSG+	CaCl2	5 | 7.5 | 10	4 | 22	None	
Lower Band	Wildtype	PEGs	CaCl2	5 | 7.5 | 10	4 | 22	None	
Lower Band	Wildtype	AmSO4	CaCl2	5 | 7.5 | 10	4 | 22	None	
Lower Band	Wildtype	PACT	CaCl2	5 | 7.5 | 10	4 | 22	None	
Lower Band	R78D/K79D	Classic	None	5 | 7.5 | 10	4 | 22	None | ATP | ADP | AMP-PNP | GTP	Behaved similar to WT, with 80% precipitates, 20% clear without substrate. With ADP, 60% of wells had precipitates and 40% of wells were clear.
Lower Band	R78D/K79D	Classic II	None	5 | 7.5 | 10	4 | 22	None | ATP | ADP | AMP-PNP | GTP	
Lower Band	R78D/K79D	JCSG+	None	5 | 7.5 | 10	4 | 22	None | ATP | ADP | AMP-PNP | GTP	
Lower Band	R78D/K79D	PEGs	None	5 | 7.5 | 10	4 | 22	None | ATP | ADP | AMP-PNP | GTP	
Lower Band	R78D/K79D	AmSO4	None	5 | 7.5 | 10	4 | 22	None | ATP | ADP | AMP-PNP | GTP	
Lower Band	R78D/K79D	PACT	None	5 | 7.5 | 10	4 | 22	None | ATP | ADP | AMP-PNP | GTP	

Protein	WT/Mut	Screen	Additive(s)	Concentration(s) (mg/mL)	Temperature (°C)	Substrate(s)	General Observation
Lower Band	E40K/D41K/E43K	Classic	None	2.5 | 5	4 | 22	None | ATP | ADP | AMP-PNP	Could not concentrate to above 6 mg/mL due to insolubility. About 95% of wells had precipitates and only 5% were clear. The nucleotides did not help with solubility.
Lower Band	E40K/D41K/E43K	Classic II	None	2.5 | 5	4 | 22	None | ATP | ADP | AMP-PNP	
Lower Band	E40K/D41K/E43K	JCSG+	None	2.5 | 5	4 | 22	None | ATP | ADP | AMP-PNP	
Lower Band	E40K/D41K/E43K	PEGs	None	2.5 | 5	4 | 22	None | ATP | ADP | AMP-PNP	
Lower Band	E40K/D41K/E43K	AmSO4	None	2.5 | 5	4 | 22	None | ATP | ADP | AMP-PNP	
Lower Band	E40K/D41K/E43K	PACT	None	2.5 | 5	4 | 22	None | ATP | ADP | AMP-PNP	
Lower Band	N181D/K186D	Classic	None	5 | 7.5 | 10	4 | 22	None | ATP | ADP | AMP-PNP	Behaved similar to the doublet, 80% of wells contained precipitates, and 20% were clear. There was no phase separation. Wells with ADP have better solubility, with 75% of wells containing precipitates and 25% clear.
Lower Band	N181D/K186D	Classic II	None	5 | 7.5 | 10	4 | 22	None | ATP | ADP | AMP-PNP	
Lower Band	N181D/K186D	JCSG+	None	5 | 7.5 | 10	4 | 22	None | ATP | ADP | AMP-PNP	
Lower Band	N181D/K186D	PEGs	None	5 | 7.5 | 10	4 | 22	None | ATP | ADP | AMP-PNP	
Lower Band	N181D/K186D	AmSO4	None	5 | 7.5 | 10	4 | 22	None | ATP | ADP | AMP-PNP	
Lower Band	N181D/K186D	PACT	None	5 | 7.5 | 10	4 | 22	None | ATP | ADP | AMP-PNP	
Lower Band	Wildtype	Classic II A11	Hampton Additive	2.5 | 5 | 7.5 | 10 | 15 | 20	4 | 22	None	50% clear, 40% phase separation, and 9 wells had hexagonal objects.
ΔY266	Wildtype	Classic	None	5 | 7.5 | 10	4 | 22	None	60% precipitates, 40% clear, the TCEP and/or the truncation might have helped with solubility.
ΔY266	Wildtype	Classic II	None	5 | 7.5 | 10	4 | 22	None	
ΔY266	Wildtype	JCSG+	None	5 | 7.5 | 10	4 | 22	None	
ΔY266	Wildtype	PEGs	None	5 | 7.5 | 10	4 | 22	None	
ΔY266	Wildtype	AmSO4	None	5 | 7.5 | 10	4 | 22	None	
ΔY266	Wildtype	PACT	None	5 | 7.5 | 10	4 | 22	None	

Protein	WT/Mut	Screen	Additive(s)	Concentration(s) (mg/mL)	Temperature (°C)	Substrate(s)	General Observation
ΔY266	R78D/K79D	Classic	None	5 | 7.5 | 10	4 | 22	None | ADP	60% precipitates, 40% clear, the TCEP and/or the truncation might have helped with solubility. The addition of ADP improved solubility to about 50% precipitates and 50% clear.
ΔY266	R78D/K79D	Classic II	None	5 | 7.5 | 10	4 | 22	None | ADP	
ΔY266	R78D/K79D	JCSG+	None	5 | 7.5 | 10	4 | 22	None | ADP	
ΔY266	R78D/K79D	PEGs	None	5 | 7.5 | 10	4 | 22	None | ADP	
ΔY266	R78D/K79D	AmSO4	None	5 | 7.5 | 10	4 | 22	None | ADP	
ΔY266	R78D/K79D	PACT	None	5 | 7.5 | 10	4 | 22	None | ADP	
ΔK269	Wildtype	Classic	None	5 | 7.5 | 10	4 | 22	None	65% precipitates, 45% clear, the TCEP and/or the truncation might have helped with solubility.
ΔK269	Wildtype	Classic II	None	5 | 7.5 | 10	4 | 22	None	
ΔK269	Wildtype	JCSG+	None	5 | 7.5 | 10	4 | 22	None	
ΔK269	Wildtype	PEGs	None	5 | 7.5 | 10	4 | 22	None	
ΔK269	Wildtype	AmSO4	None	5 | 7.5 | 10	4 | 22	None	
ΔK269	Wildtype	PACT	None	5 | 7.5 | 10	4 | 22	None	